Development of A Coupled Rainfall-Runoff and Inundation Model for Flood Forecasting Using Satellite and ECMWF Data

TIAN HUANG

February, 2018

SUPERVISORS:

Dr. Ing. T.H.M Rientjes
Prof. Dr. V.G. Jetten

Development of A Coupled Rainfall-Runoff and Inundation Model for Flood Forecasting Using Satellite and ECMWF Data

TIAN HUANG

Enschede, The Netherlands, February, 2018

Thesis submitted to the Faculty of Geo-Information Science and Earth Observation of the University of Twente in partial fulfilment of the requirements for the degree of Master of Science in Geo-Information Science and Earth Observation.
Specialization: Water Resources and Environmental Management

SUPERVISORS:
Dr. Ing. T.H.M Rientjes
Prof. Dr. V.G. Jetten

THESIS ASSESSMENT BOARD:
Prof. Dr. Z. Su (Chair)
Prof. Dr. P. Reggiani (External examiner)
Dr. Ing. T.H.M Rientjes (First supervisor)
Prof. Dr. V.G. Jetten (Second supervisor)

ABSTRACT

In this study an integrated rainfall-runoff – inundation model and a flood forecasting procedure has been developed for Nyabugogo catchment and Kigali city in particular. The study area has a size of 454 km^2. In recent years, Kigali city in Nyabugogo catchment has suffered from frequent flooding. Recent flood simulation studies in the area were based on the 1D2D hydrodynamic flood model. For those studies boundary inflow discharges have been simulated by the lumped HEC-HMS rainfall-runoff model. In this study, OpenLISEM model approach has been used that is a fully distributed model designed to simulated overflow runoff and related flooding. OpenLISEM is able to simulate spatially distributed patterns of model inputs that, for this study, are represented at grid resolution of 90 m × 90 m. For runoff and flood simulation purposes, bias corrected CMORPH rainfall estimates have been used as meteorological forcing inputs. Catchment characteristics required by the OpenLISEM, such as DEM, soil properties, and channel network, were mostly collected from global databases or adopted from previous studies. Four 2-day flooding events have been simulated in this study. By absence of gauged streamflow time series, for model calibration the simulated streamflow by the HEC-HMS model served as target. Optimized model parameters served simulation of all four events as well as flood forecasting procedure. For forecasting, ECMWF precipitation forecasts are tested that were merged with corrected CMORPH rainfall estimates. The performance of the forecasts was assessed with lead times from 12 to 48 hr.

With respect to CMORPH rainfall estimates, findings on bias correction method show that the Time Variable method with window length of three days is best performing. For model calibration, the RVE of four events is 11.47%, 7.30%, -0.72%, and 8.70%, respectively. With reference to previous HEC-HMS simulation results, the difference in the magnitude of maximum streamflow discharge is acceptable (mean -27.84%) but with some differences in peak time delay. Most inundated area created by the OpenLISEM simulation is from effects by accumulated rainfall and depressions in local scale, while no clear flooding was shown as a result of channel bank inundation. Generally, the OpenLISEM is able to simulate the outlet streamflow discharge but not the inundation in Kigali city in this study. The distribution of the channel network, the depth of subsurface soil layer, and the initial moisture content are the most important model inputs and have large effect on the model results. In flood forecasting, the average RMSE of for four events with lead times from 12 to 48 hr is 171.4, 1119.2, 1027.5, and 4895.6 m^3/s, respectively. The overall performance of flood forecasting is considered acceptable but not excellent. Only few forecasted hydrographs can fit the simulated counterparts well while the performance of the rest forecasts is not satisfactory. It was revealed that the accuracy of the forecasts does not decline considerably as lead times increase, this presumably by effects of the relatively short lead times (12 to 48 hr) and short forecasting interval (12 hr).

Keywords: OpenLISEM, distributed model, CMOPRH, flood forecasting, ECMWF

ACKNOWLEDGEMENTS

I would like to firstly express my gratitude to my dear parents, who have given me unconditional love and support during my study. Thank you.

I would like to express my gratitude and respect to my first supervisor Dr. Tom Rientjes for his guidance and encouragement. You have helped me a lot in improving my research and writing skill and widening my knowledge.

I would also like to extend my gratitude to my second supervisor Prof. Victor Jetten for his professional comments and advices in technical issues.

I would like to thank all the people who have helped me during my thesis work and my study.

TABLE OF CONTENTS

LIST OF FIGURES

LIST OF TABLES

1. INTRODUCTION

1.1. Background

A flood is an overflow of water that inundates land that is usually dry. Floods frequently occur in a global scale and account for about one-third of global natural hazards (Cosgrove & Rijsberman, 2014). Effects of flood disasters, including economic and societal damage, have a tendency to worsen over time. Compared to geological catastrophes, weather-related disasters including floods have shown a more significant rising both in numbers and in financial losses over recent years (Romang et al., 2011). Flood events can result in extremely dire consequences, not only for environmental systems but also to stability of human societies.

In urban areas, floods often cause serious problems. Flood events damage buildings and may make thousands of citizens homeless. Poor drainage systems also contribute to damages because of insufficient drainage capacity. In fact, most modern cities suffer from floods when heavy storms occur. In some developing countries, the situation becomes even worse when cities expand at high speed but still rely on existing drainage systems without improvement and extension (Mark, Weesakul, Apirumanekul, Aroonnet, & Djordjević, 2004). Therefore, a number of governments and organizations around the world are making efforts on reducing the losses on lives and finance caused by floods. Various solutions and projects, such as FLOODsite, Flood Control 2015, and International Levee Handbook, aim to build and improve flood protection systems and constructions to minimize the consequences of flood events (Krzhizhanovskaya et al., 2011).

Rwanda, known as the "Country of a Thousand Hills" because of its mountainous topography, is one of the countries suffering from frequent flood events. Floods, mostly riverine floods and flash floods are severe threats to Rwanda since it has steep hills, dense river network and vast wetlands. Kigali city, the capital of Rwanda, has experienced not only frequent but also more extreme floods since the 2000s because of climate, location, topography and inadequate drainage systems. floods commonly are flash floods that are of short time period. Floods commonly only last from several hours but also could last few days depending on rainfall patterns that cause the flooding. In 2006, 27 percent of buildings in Kigali City were located in flood-prone areas, on which the residents, infrastructure, and social activities were endangered because of flash floods (Habonimana, Bizimana, Uwayezu, & Tuyishimire, 2012). The economic and social values of this area and its vulnerability to flash floods are the main reasons for choosing Kigali City as the area of interest for the study.

Some measures have been taken to reduce the consequences of flash floods. For example, relocation of residential buildings and infrastructure was operated in Kigali city base on the flood risk analyses done by Bizimana & Schilling (2010). It is necessary to understand the characteristics of floods before taking actions on flood management. Therefore, numerical models can be a suitable option in flood risk analysis and management through simulation and prediction in channels and floodplain (Horritt, Di Baldassarre, Bates, & Brath, 2007).

Flood forecasting is one of the practical solutions to the development of flood mitigation measures. It is able to provide an alarm or early warning of potential floods few hours or days in advance, so to allow for evacuation, temporary construction and other measures to reduce the effects of floods. Hydrological models are commonly used in the flood forecasting procedure. According to UNISDR (2002), rainfall-runoff model may be needed to provide runoff estimates but also more complex models with coupled channel flow and overland flow runoff models may be needed in flood studies. Whereas a lumped rainfall-runoff model requires relatively few data and only provides channel runoff as model output, a distributed model requires much more data but offers more details about runoff production in the upstream area but also may provide flood extent in the flood prone area.

1.2. Literature Review

1.2.1. Flood Modelling

There are many definitions of "a model", most of which state that a model is a simplified representation of real world for specific purposes. According to Rientjes (2015), a "hydrologic model" is "a simplified representation of a (part of) hydrologic system by means of a mathematical model, model parameters, state-variables, meteorological stresses and possibly boundary conditions". Figure 1.1 illustrates a diagram of the inputs required for a numerical physically based hydrologic model.

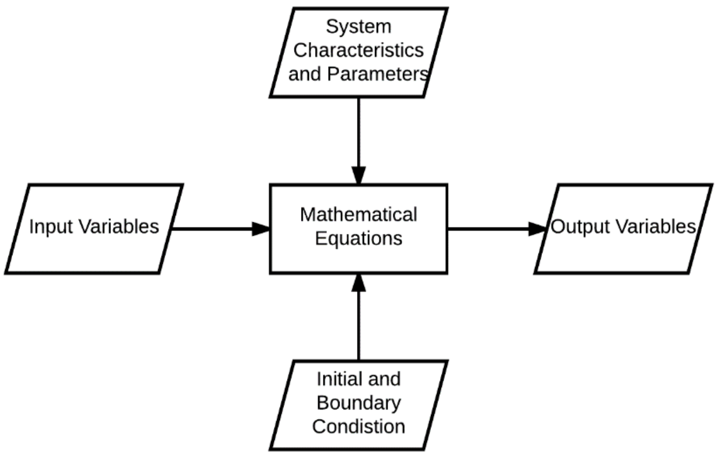

Figure 1.1 Diagram of a numerical physically based hydrologic model. Source: Rientjes (2015).

Modelling in urban areas is complicated, mainly because of the complex topography of a city and the fact that it is complicated to represent geometry of buildings and infrastructure. To overcome the latter, assumptions can be made that water flows on the roads and the junctions when a major flood event occurs in a dense city (Mignot, Paquier, & Haider, 2006). Furthermore, in many less developed countries measurements on runoff and streamflow discharges as well as observation on flood characteristics are not available, complicating calibration and validation of a model. Therefore, an adequate assessment of the performance of a hydrological model becomes one of the major problems for model development.

The flood model used in this study is the Limburg Soil Erosion Model (LISEM), which is a physically based flood model that also can simulate soil erosion. The model is a flash flood model that simulates infiltration excess runoff for extreme rainfall events. Interflow and/or rapid subsurface flow are not considred as runoff constributig processes. OpenLISEM, an open source model adapted from de Roo, Wesseling, & Ritsema (1996), is able to simulate hydrologic processes and sediment processes during a single rainfall event within a catchment. Figure 1.2 indicates the model structure only containing the hydrologic processes since the sediment processes were not taken into account in the study. In simulating ruoff, a part of rainfall becomes interception whereas the rest reaches the ground. Rainwater can eather be stored in the subsurface soil layer by means of infiltration, or be stored by effects of depressions and high surface roughness. Rainfall becomes Hortonian overland flow when rain rate exceeds infiltration rate, that also can be. when the soil layer is saturated. Overland flow joins channels in the lowest part of simalated local scale subcatchments so to result in channel flow. Flow equations used in computing these hydrologic processes can be found in Baartman, Jetten, Ritsema, & de Vente (2012).

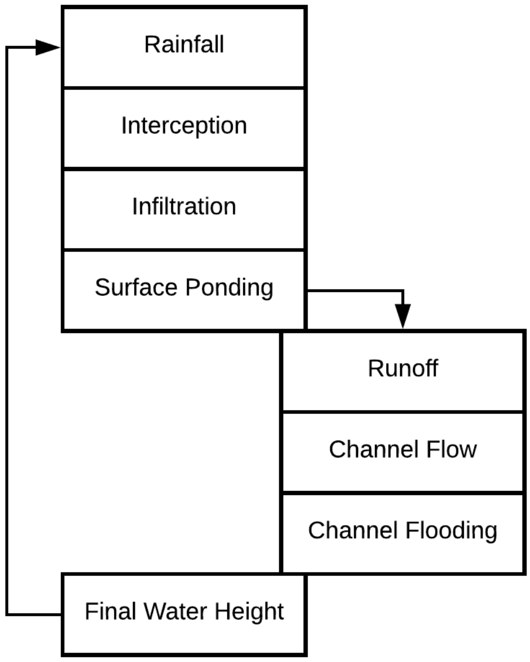

Figure 1.2 Flow chart of hydrologic processes in the OpenLISEM. Source: Bout & Jetten (2018)

The simulation of water flow plays an essential role in flood modelling. In the OpenLISEM software (version 3.96) three approaches of flow approximations are applied that are , 1) channel flow follows a 1D kinematic wave, 2) flooding from the channels follows a 2D dynamic wave and 3) both 1D knimatic wave and 2D diffusive wave can be selected for overland flow approximation (Jetten & van den Bout, 2017). When 1D knimatic wave is selected, a flow network was created from DEM map. The flow direction for each cell only depends on the topographic slope and is fixed during simulation. Diffusive wave approximation takes the water depth into account but only solves mass balance and neglects inertial terms in computation. Dynamic wave solves both mass balance and momentum balance, which is necessary in shallow water simulation.

In the last version of 'OpenLISEM Harzard' (i.e., 1.0), which is used in this study, some changes in flow approximations have been made. At present channel flow follows 1D diffusive wave, and both overland flow and flood inundation follow a 2D dynamic wave. Therefore, there is no distinction in the compution principles of overland flow and flooding, and the water depth on the land surface represents the depth of flooding. The equations of the three flow approximations and the difference among them is explained in Bout & Jetten (2018).

In recent years LISEM has been used for flash flood simulation in several studies in Kampala, Uganda. Sliuzas, Flacke, & Jetten (2013) studied the effect of urbanization on flooding in Lubigi catchment (28 km^2) in Kampala, in which a 1:10 year rainstorm was simulated using an observed rainfall event. The maximum rain intensity during the rainstorm is over 100 mm/h. Mhonda (2013) used LISEM in the same area and set it up with spatial resolution as 10 m, simulation period as 500 min, and time step as 10 sec. Habonimana (2014) did some further work in the same areaand run the model with spatial resolution as 20 m, simulation period as 2300 min, and time step as 10 sec. The simulation period was set longer to allow almost all the runoff caused by the intense rainfall to reach the outlet. Both studies applied fine spatial resolution for an ideal representation of urban elements. A rain gauge located in the city was the main source of rainfall data available. Simulations with rainfall estimates from Weather Research Forecast (WRF) model with 10 min temporal resolution and 1 km spatial resolution was used in this study as well.

Previous ITC students have contributed to the work of flood simulation and analyses in Kigali city. Manyifika (2015) developed a rainfall-runoff model for the upstream areas to the actual flood prone area in Kigali for which high resolution (5-20 m) 1D2D SOBEK models were developed. Whereas for the for runoff simulation in Nyabugogo catchment a HEC-HMS model was developed and calibrated using observed rainfall and discharge in the period 2011-2013, for the commercial hub of Kigali city the 1D2D SOBEK flood inundation model was developed. Ali (2016) further developed the 1D2D SOBEK model and assessed the effects of urbanisation and infrastructure on flooding.

1.2.2. Satellite Rainfall Estimates (SREs)

Satellite products, such as Climate Prediction Center Morphing Technique (CMORPH), Tropical Rainfall Measuring Mission (TRMM) Multisatellite Precipitation Analysis (TMPA), and Precipitation Using Artificial Neural Networks (PERSIANN) can provide spatially variable rainfall data in near-global scale. For instance, CMORPH is able to provide rainfall data with 8 km spatial resolution at the equator and 30 minutes temporal resolution.

All the rainfall data from satellites products contain uncertainties. Several studies intercompared SREs for the east Africa region with outcome that CMORPH proved to be more accurate to represent the gauge rainfall compared to products from, e.g., TRMM, TMPA or PERSIANN. Haile, Habib, & Rientjes (2013) described that CMORPH is widely used in hydro-meteorological applications around the world because of its high temporal and spatial resolutions. Habib, Haile, Sazib, Zhang, & Rientjes (2014) concluded that CMORPH is a suitable product to estimate rainfall for simulation of flood events. However, studies show that rainfall estimations from satellite products are prone to error (i.e., bias) resulting from systematic and random errors.

To identify a suitable satellite rainfall product to represent rainfall distributions in the Nyabugogo, and neighbouring catchments, Sendama (2015) performed a study on CMORPH, Rainfall Estimates (RFE) 2.0 and TRMM 3B42 v7 products and concluded that CMORPH is preferred since it best represented in-situ based rainfall patterns. Sendama (2015) showed that for the period 2009-2013 a bias factor of 0.67 (the ratio between accumulative daily SREs and accumulative daily in-situ measurements) and a mean error with -1 mm/day compared to in-situ measurements. In the rain gauges overlapping with this study

(Gitega, Kigali_aero, and Cyinzuzi), the overall bias is 0.82, 0.85, and 0.61 respectively. As such, CMORPH only shows little underestimation of in-situ based rain estimates. By these findings CMORPH was selected for use in this study.

1.2.3. Weather Forecasting Products

Global ensemble forecasting systems are able to provide weather forecasts including rainfall forecasts. For instance, the European Center of Medium-range Weather Forecasting (ECMWF) can provide weather forecasts including rainfall at 0.25° spatial resolution and 6 hr temporal resolution with lead times from 0 to 10 days (ECMWF Directorate, 2012). Buizza et al. (2005) compared the weather forecasting results based on ECMWF, the Meteorological Service of Canada (MSC0), and the National Centers for Environmental Prediction (NCEP), which are all weather forecasting systems. Though none of them can fit the reality reliably, the overall performance of ECMWF was considered the best.

Haile, Tefera, & Rientjes (2016) developed a simple flood forecasting model for the Benue basin of 918,872 km^2 (Niger river basin) through HEC-HMS simulation using ECMWF rainfall forecasts. Rainfall estimates preceding the flood forecast window was represented by Tropical Rainfall Measuring Mission (TRMM), this by lack of in-situ rainfall data. The simulated stream flow discharges were compared to the observed counterparts during the flood events. With the lead times from 1 to 6 days, ECMWF rainfall forecasts were possible to provide moderately accurate results in flood forecasting for Benue basin.

Roulin & Vannitsem (2005) developed hydrological prediction system using a water balance model to simulate streamflow at a storm event with lead times from 1 to 9 days. The model was developed for the Demer catchment of (1775 km^2) and the Ourthe catchment (1616 km^2) in Belgium and was with two rainfall inputs: ECMWF rainfall forecasts and historical observed rainfall on the same calendar dates with the storm event in the past 30 years. Compared to the results based on historical observation, the results based on ECMWF forecasts were proved to perform better.

Benninga (2015) assessed the performance of streamflow forecasting using lumped HBV rainfall-runoff model for the Biała Tarnowska river catchment of 956.9 km^2. ECMWF rainfall forecasts and historically observed rainfall on the same calendar dates with the event served as meteorological inputs respectively. Low, medium, and high flows were defined according to discharge thresholds with the exceedance probability of 75% and 25% compared to the observed discharge of past years. Historically observed rainfall performed better in the low flow forecasts, while ECMWF forecasts provided better results in the high flow forecasts. In terms of flooding forecasting, ECMWF were probably better inputs as flooding is associated with high streamflow. The performance of forecasting is generally the best for lead times of 2 to 5 days.

1.2.4. Digital Elevation Model (DEM) Map

Availability of an accurate Digital Elevation Model is prerequisite to the development of a flood model. A DEM map with a suitable resolution and a good accuracy can be a good representation of the topography in the study area used in flood modelling. Evaluation on a DEM map can is on the accuracy of its geolocation and elevation, e.g. by field surveying as shown in Ali (2016) for Kigali flood prone area.

Commonly used elevation models in flood modelling are the Shuttle Radar Topography Mission (SRTM) DEMs and the Advanced Spaceborne Thermal Emission and Reflection Radiometer (ASTER) DEMs.

SRTMs are available at 90 and 30 m spatial resolution from 60 degrees north latitude to 54 degrees south latitude (Van Zyl, 2001). Rodriguez, Morris, & Belz (2006) did a global assessment on the performance of SRTM and showed absolute geolocation error, absolute height error, and relative height error in Africa of respectively 11.9 m, 5.6 m, and 9.8 m with 90% confidence.

The Advanced Spaceborne Thermal Emission and Reflection Radiometer (ASTER) provides a DEM with 30 m spatial resolution along the tracks of spacecraft. Fujisada, Bailey, Kelly, Hara, & Abrams (2005) evaluated its geolocation and vertical accuracy and got the value of better than 50 m and about 20 m respectively. The root-mean-square error (RMSE) of ASTER is ± 8.6 m claimed by US Geological Survey (USGS) (Hirano, Welch, & Lang, 2003).

Schumann et al. (2008) assessed the performance of DEM from LiDAR, contours and SRTM in deriving water stages and suggested a lower accuracy of SRTM than the other two. Nevertheless, for large and homogeneous floodplains, SRTM is still a potential DEM source in initial vital flood simulation due to its moderately good accuracy. Jarihani, Callow, McVicar, Van Niel, & Larsen (2015) applied SRTM and ASTER in hydrodynamic modelling and concluded that they are suitable products for data poor areas after calibrated and validated using control point dataset.

1.2.5. Land Surface Properties

In distributed rainfall-runoff modelling, surface properties representations often serve estimation of interception, micro storage and surface flow (both channel flow and overland flow). Different values on properties can be applied to different land cover type according to Jetten & van den Bout (2017).

Manning's n is an essential parameter used in Manning's Equation to compute the flow velocity and discharge on the slope surface and in the channel. It represents the resistance of the surface and is one of the most effective parameters in surface flow modelling. Chow (1959) and West Sacramento City Hall (2002) provided tabulated values of Manning's n for specific land cover types in floodplain and channel types. It is noticeable that the Manning's n values of both surface and channels are not pre-set or static and can be optimized during the model calibration.

Random roughness is a coefficient used in empirical equations to compute maximum water storage at local depressions, which can store water before it becomes overland flow. To measure random roughness is costly, labor intensive and time-consuming thus roughness values often are defined by model sensitivity and calibration procedures. Mwendera & Feyen (1992) found an empirical relation between Manning's n and random roughness from statistical methods. Onstad (1987) claimed that apart from the soil type, several factors have effects on the random roughness as well, especially tillage and rainfall.

1.2.6. Soil Properties

In this study, the infiltration process is simulated using Green and Ampt (Green & Ampt, 1911) approximation. It assumes that soil properties do not change in the vertical direction. The soil above the wetting front is saturated while the soil below is not and a sharp wetting front results. For modelling the initial soil moisture content need to be defined and set. For calculation of infiltration, soil properties, including saturated hydraulic conductivity, porosity, average suction at the wetting front, and initial volumetric soil moisture content, are main inputs required by the method. (descriptions modified after Mein & Larson (1971))

The difficulty to set initial soil moisture content of the unsaturated soil layer in the OpenLISEM constitutes a major source of uncertainty in hydrological modelling. This since spatially distributed pattern of the initial soil moisture content as required by the model is not available and thus a substantial obstacle in the procedure of model initialization (Noto, Ivanov, Bras, & Vivoni, 2008). In this study, the initial soil moisture content was firstly set to 0.7 of the porosity and adjusted in the later tests.

Due to the lack of field measurements related to the hydraulic properties of the soil in the study area, global soil databases became the major sources of soil information in this study. SoilGrids is a data archive system combining publicly available soil profile data and remote sensing data. It can provide several estimations of numeric soil properties and soil classification based on the World Reference Base (WRB) and United States Department of Agriculture (USDA) classification systems in a global scale with 250 m resolution (Hengl et al., 2017).

The Food and Agriculture Organization of the United Nations (FAO) soil database was established from a statistical analysis of the 4353 soil profiles. Global maps are available at a scale of 1 to 5 million. It contains some soil physical and chemical properties, most of which in topsoil (0-30 cm) and subsoil (30-100 cm) (Batjes, 1997). After collaborated with other databases, it is now known as the Harmonized World Soil Database with a spatial resolution of approximately 1 km at the equator. It was obtained from many sources and comprehensive (Jones & Thornton, 2015).

Based on the surveys and analyses of soil samples, Rawls, Brakensiek, & Miller (1983) provide the parameter values needed in Green and Ampt infiltration equation for different types of soil. Saxton & Rawls (2006) also provided tabulated properties for different soil types through laboratory experiments. Besides, they developed Soil Water Characteristics, a computer program which aims to transfer soil texture to soil classification and provide physical and chemical properties based on experiments ("Soil Water Characteristics," n.d.).

2. OBJECTIVES, RESEARCH QUESTIONS AND STUDY AREA

2.1. Problem Statement

Kigali city has experienced frequent flash floods in recent years that shortly developed (2-6 hr) after a rainstorm occurred. An understanding on characteristics of floods and catchment runoff behaviour is needed for development of flood mitigation measures or early warning. As such development of a hydrological model in this area is relevant but not trivial. For the study area, the hydro-meteorological in-situ data is not only scarce, but data also is of poor quality. The lack of in-situ data especially with respect to river geometry, soil properties, and flood extent is a main obstacle. Hence, remote sensing and global databases are alternatives to obtain the catchment and meteorological information needed for modelling.

Previous flood modelling in Kigali city was based on 1D2D SOBEK model, with simulated catchment runoff from the separate HEC-HMS model that served to estimate the river inflow to the flood model domain. The estimated runoff hydrograph from HEC-HMS served as the SOBEK inflow boundary condition for the flood events. HEC-HMS is a conceptual rainfall-runoff model ignoring spatial variability and rainfall-runoff relation in each sub-catchment was obtained using simple methods. Reference is made to Manyifika (2015) and Ali (2016) for detailed description on the approaches. To overcome the limitations of such approach, a distributed, integrated rainfall-runoff – inundation model is required to simulate spatially distributed patterns of meteorological inputs, catchment characteristics, and hydrological processes. Besides, an integrated rainfall-runoff – flood inundation model that solves the combined model water balance, such approach would enable to represent in respective time and space domains the hydrological and flow processes during a flood event.

With the help of rainfall data from different sources (in-situ measurements, remote sensing, and meteorological forecasts) for runoff modelling, it could serve flood simulation as well as flood forecasting. For the area observations on floods are essentially absent, so the flood assessments in this study and LISEM model approach focused on comparing model performance to previous simulation results in Manyifika (2015) and Ali (2016). It is noted that results in both studies could not be verified by detailed and accurate field observations but the overall patterns on flood dynamic were not considered unrealistic by respective researches with expert knowledge on the area. As such for this study discharge and flood extend results provided by Manyifika (2015) and Ali (2016) served as a benchmark for assessing simulation results in this study that are for the same events. The accuracy of flood forecasting was evaluated when rainfall data from various sources were selected as inputs.

2.2. Objectives

The main objective of this study is to develop an integrated rainfall-runoff – inundation model and a flood forecasting procedure for Kigali city with possible rainfall inputs from in-situ measurements, remote sensing products and weather forecasts.

The specific objectives are:

- To assess the performance of CMORPH rainfall estimates and ECMWF rainfall forecasts using in-situ measurements,
- To correct the biases of CMORPH rainfall estimates based on in-situ measurements,
- To develop and calibrate a rainfall-runoff – inundation model simulating historical flooding events using OpenLISEM simulation,
- To evaluate the performance of the flood forecasts when ECMWF rainfall forecasts combined with CMORPH estimates serve as meteorological inputs.

2.3. Research Questions

The research questions are:

- What bias correction scheme is the most effective for flood modelling purposes?
- What are the most sensitive parameters and settings in the OpenLISEM model?
- What is the performance of the model in simulating historical flooding events?
- What are the potentially inundated areas according to simulation?
- What are the main sources of uncertainty in model development?
- How to evaluate flood forecasting model performance?
- How is flood forecasting performance affected by increasing forecasting lead times (12 to 48 hr)?
- How does the uncertainty in rainfall forecasts affect the accuracy of flood forecasting?

2.4. Study Area

Rwanda is in the central eastern part of Africa, between 1 degree south latitude and 3 degrees south latitude, 29 degrees east longitude and 31 degrees east longitude. The size of Rwanda is 26338 km^2. It is a mountainous country and has a high elevation in the entire country with the lowest point at 950 m a.s.l.

Nyabugogo catchment is a major catchment covering the central, eastern, and northern part of Rwanda. The area of Nyabugogo catchment is 1661 km^2 including lake Muhazi. Kigali city, the capital of Rwanda, is located at the downstream of Nyabugogo catchment with the most densely urbanized area with high population. Nyabugogo river, the main river in the catchment, starts from lake Muhazi and flows through the commercial hub of Kigali city where it causes flooding. The entire catchment is divided into 12 sub-catchments including the floodplain where Kigali city is located in. Considering the area for the model, 9 sub-catchments with a total area of 454 km^2 was selected as study area. Figure 2.1 shows the location of Nyabugogo catchment and the study area.

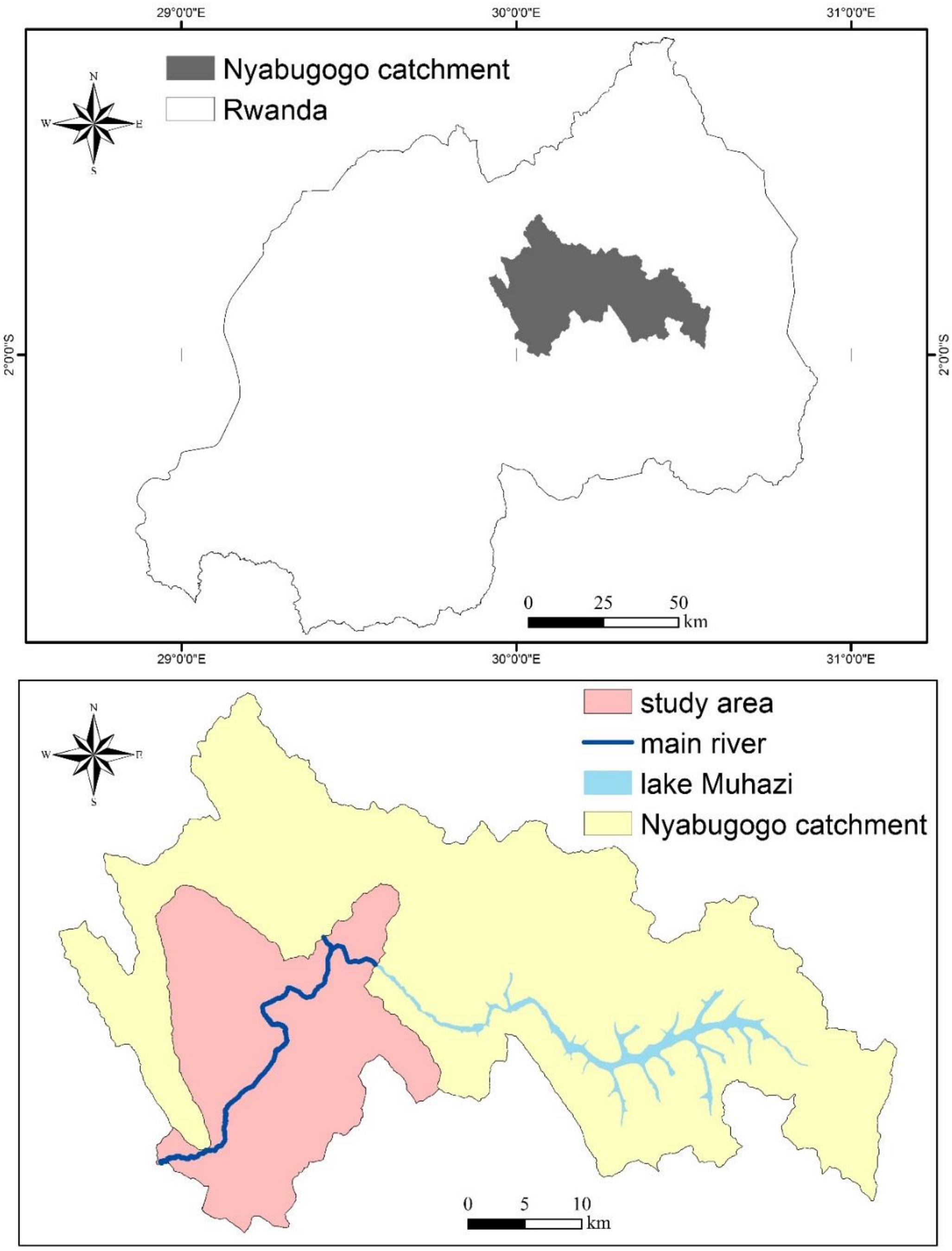

Figure 2.1 Study area.

3. DATA AND METHODOLOGY

3.1. Conceptual Framework

For this study a coupled rainfall-runoff and inundation model and flood forecasting procedure must be developed for Kigali city and Nyabugogo catchment using OpenLISEM simulation. Figure 3.1 illustrates the main steps of this study. Rainfall estimates from CMORPH and ECMWF were utilized as the meteorological forcing in flood simulation and forecasting procedure after bias correction based on in-situ rainfall measurements. Data representing catchment characteristics were adopted from Manyifika (2015) and Ali (2016) and further collected from global databases. The observed and simulated discharge data during flooding events served in developing and calibrating the model. Forecasting results were compared to the previous simulation after calibration.

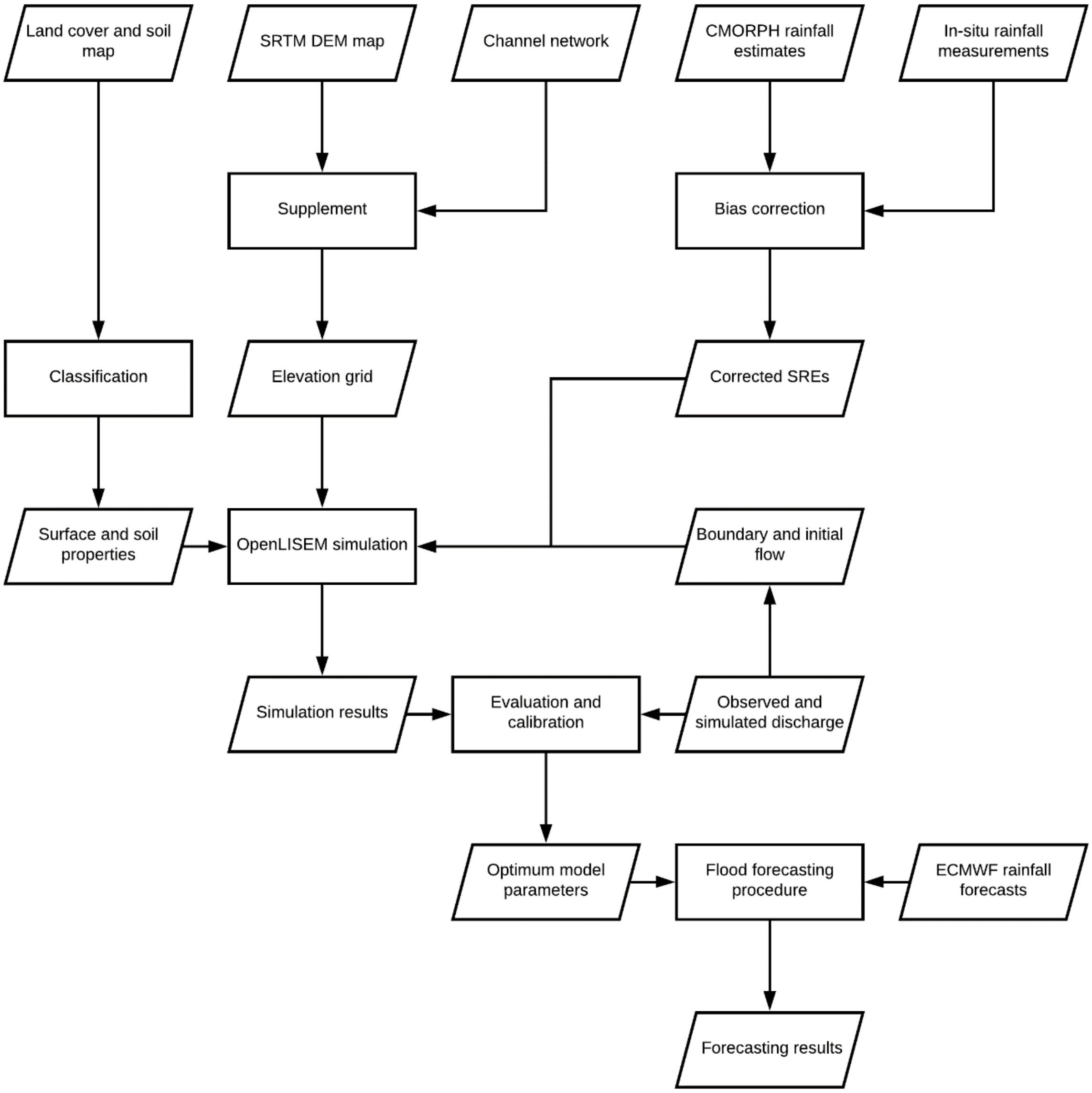

Figure 3.1 Flow chart of methodology.

3.2. Data Processing

3.2.1. Rainfall

Rainfall data obtained from in-situ measurements are typically considered as the most accurate and representative data of the catchment. In-situ rainfall data was collected by Manyifika (2015) from Rwanda Meteorology Agency (WMA). Four rain gauges in or close to the study area (Gitega, Kigali_aero, Rubungo, and Cyinzuzi) were selected using Thiessen polygons to represent spatial distribution of rainfall. The time series of all the selected gauges is from 2009 to 2013 with a daily interval. In this study, recorded in-situ rainfall measurements that caused reported flooding situations mainly served to correct rainfall data from other sources. Figure 3.2 indicates the location of these four gauges and the areas they represent.

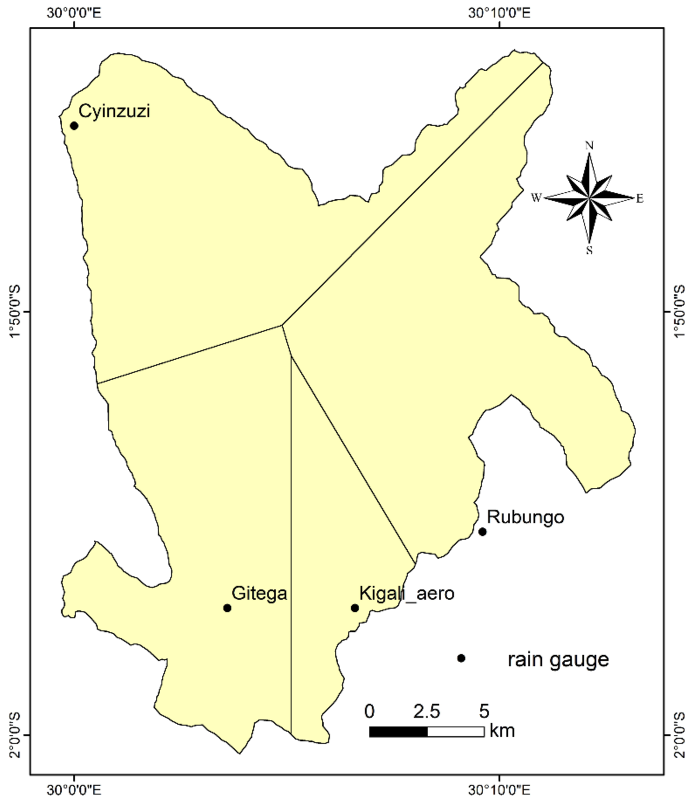

Figure 3.2 Location of four selected rain gauges and the area they represent using Thiessen polygon. Source: Manyifika (2015).

Given the size of the basis area, the temporal resolution of the in-situ rainfall (i.e. daily) is too coarse to meet the demand of flood simulation and forecasting purposes. Thus, sub daily rainfall estimates from CMORPH were selected to represent the distributed rainfall during the extreme events due to its better spatial and temporal resolution compared to other satellite products. CMORPH data was downloaded through ISOD toolbox in ILWIS software with 8 km spatial resolution and 30 min temporal resolution.

In the flood forecasting procedure, precipitation forecasts from ECMWF were used as the rainfall inputs. They were downloaded on http://apps.ecmwf.int/datasets/data/tigge/levtype=sfc/type=cf/ with 0.25° spatial resolution and 6 hr temporal resolution. The precipitation forecasts were released twice in a day, at 00:00 and 12:00.

3.2.2. Discharge and Flooding Events

The Yanze and Rusumo sub-catchment, the lake Muhazi sub-catchment, and the entire Nyabugogo catchment (at Nemba station located in the downstream part of Kigali) are gauged. The discharge data was collected from Rwanda Natural Resources Authority (RNRA) and Integrated Water Resources Department (IWRMD). The overlapping time series of these four discharge stations is from 2011 to 2013. Manyifika (2015) did some field work to establish and construct rating curves of the stations, making it possible to convert water level to river discharge. It is assumed that the rating cure remained the same during the flood events simulated for this study. Discharge time series of four gauging stations are indicated in Figure 3.3. The three gauged sub-catchments were excluded in this study, and the discharge data of them is used as boundary flow in the model.

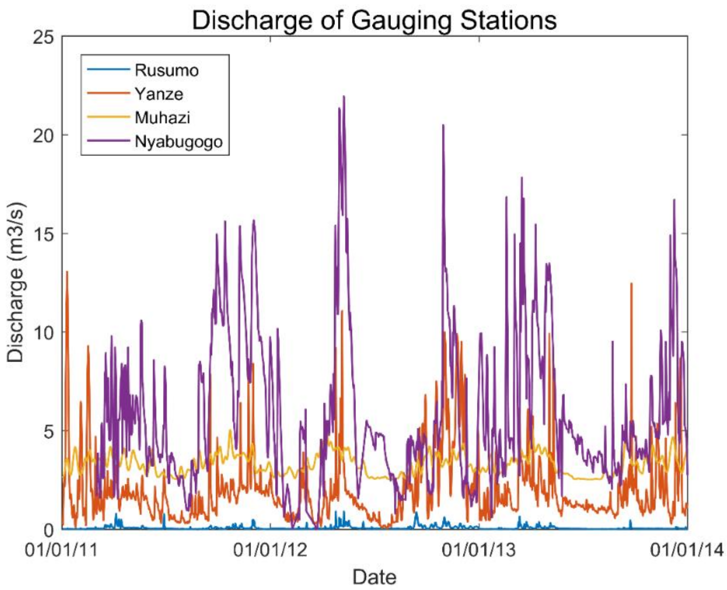

Figure 3.3 Discharge of four gauging stations from 2011 to 2013. Source: Manyifika (2015).

Manyifika (2015) selected four flooding events from 2011 to 2013 according to the peaks of hydrographs in Nyabugogo main river and rainfall values on the corresponding dates. Since the study provided simulated streamflow discharge in all sub-catchments during these events with high temporal resolution (30 min), the same events were selected in this study to transfer the simulation results to become boundary flow and base flow discharge. For each selected extreme rainfall event, the period of simulation was two days, the specific dates of them are listed below:

- 29th and 30th November 2011;
- 3rd and 4th May 2012;
- 31st October and 1st November 2012;
- 11th and 12th March 2012.

3.2.3. DEM Map

The elevation map collected from the local government proved to be not of good accuracy in the area with high altitude values. It is considered not a suitable product for the study area that contains much mountainous area. Concerning global DEM products, DEM maps from SRTM were proved to perform better than those from ASTER in some studies. Therefore, DEM maps from SRTM were selected to represent the elevation in this area. DEM maps with 30 m and 90 m resolution can be chosen. Due to the large area of the catchment and the limitation of computation time, a coarse resolution (90 m) was applied. The DEM maps from SRTM were downloaded on https://earthexplorer.usgs.gov/. The elevation of the study area ranges from 1354 m to 2237 m with the lowest elevation and the catchment outlet in the southwest part, which is indicated in Figure 3.4. It is worth mentioning that the elevation is an integer, so the distinction between two adjacent cells is also an integer. It is an obvious drawback of SRTM and might influence the results.

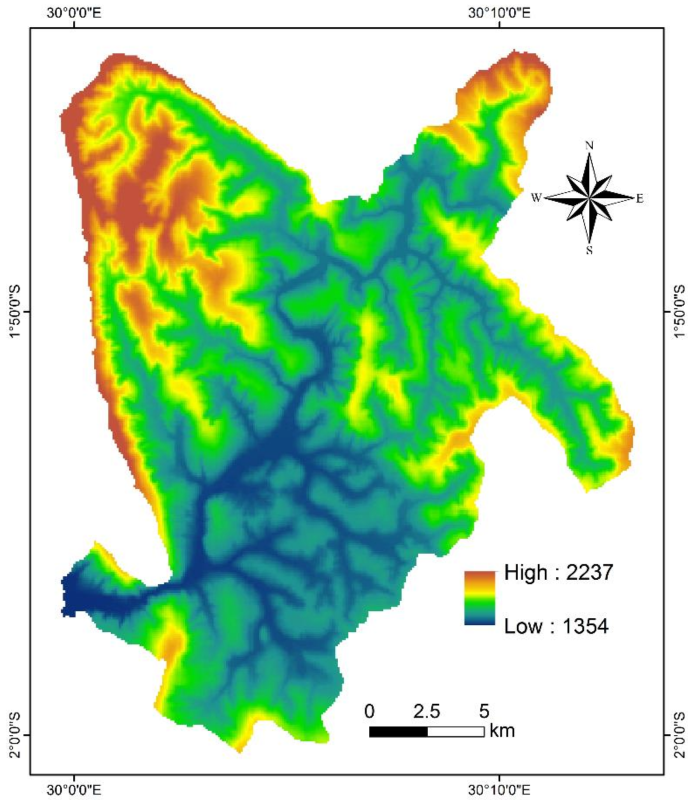

Figure 3.4 SRTM DEM map.

3.2.4. Land Cover and Surface

A base map database covering entire Rwanda was collected by Manyifika (2015) from RNRA. The base map database contains a vector land cover map. It was rasterized with 90 m resolution, which is shown in Figure 3.5. Urban area representing Kigali city is located in the south part of the study area, and the rest part is mostly covered by agricultural lands and forest. Each land cover type was given the corresponding properties, including random roughness, Manning's n, vegetation height, and fraction covered by vegetation according to the recommended values provided by Jetten & van den Bout (2017). The classification in the land cover map is slightly different from the one in the manual, so the most similar class is used when no class in the manual is the same as the land cover map.

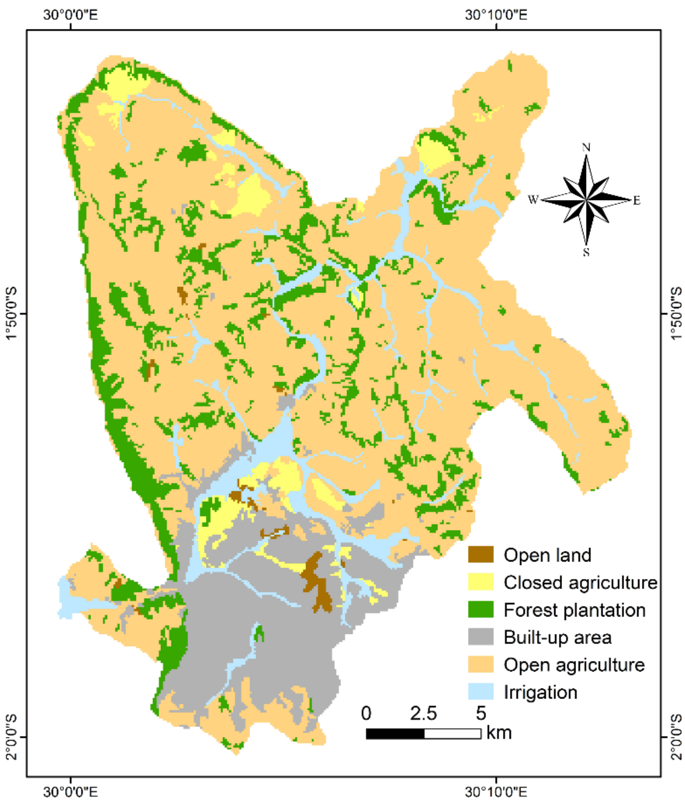

Figure 3.5 Land cover map. Source: Manyifika (2015).

The other factors describing water storage effects (i.e. Leaf Area Index (LAI) and the maximum canopy storage capacity (Smax)) are not available in the table. LAI was calculated from the fraction covered by vegetation (Cover). The equation used is below:

$$LAI = \frac{ln(1 - Cover)}{-0.4}$$

de Jong & Jetten (2007) found the statistical relation between Smax and LAI for various types of vegetation. Different empirical equations were applied to different kinds of vegetation to compute Smax from LAI. The equation of crops was applied on all the agricultural land, and the vegetation type of forest plantation area was assumed to be broadleaved forest. LAI of built-up area was very low due to its low Cover, and Smax of built-up area was set as 0. Cover, LAI and Smax of open land were all 0.

Table 3.1 Roughness and vegetation parameters

Parameter	Random roughness	Manning's n	Plant height	Cover	LAI	Smax
Unit	cm	-	m	-	-	mm
Open land	0.5	0.1	0	0	0.00	0.00
Closed agriculture	1	0.03	1	0.8	4.02	2.85
Forest plantation	1	0.1	5	0.8	4.02	1.15
Built-up area	0.5	0.05	5	0.1	0.26	0.00
Open agriculture	0.7	0.03	0.5	0.5	1.73	1.78
Irrigation	1	0.03	1	0.8	4.02	2.85

The parameters of each land cover type are indicated in Table 3.1. In LISEM, area of crusted and compacted surface involves a different set of hydraulic properties of the soil, and no infiltration process was included area of hard surface. They are ignored in this study because of the lack of detailed information. A road network containing tarred roads and untarred roads is available from the base map, in which only the tarred roads should be considered as impermeable. Regarding the road widths range in an extensive range in this study, and the number of tarred roads is too small to affect the computation of infiltration, a road network was excluded in the model due to the coarse spatial resolution of the model. Concerning Manning's n value of the main river channel, 0.048 was set in this study according to Chow (1959).

3.2.5. Soil Properties

Two global soil databases, Soilgrids and FAO, were compared to each other. Compared to FAO database, Soilgrids database has finer spatial resolution and more useful information. It was then selected, and soil data was downloaded on http://www.soilgrids.org/ provided at 250 m * 250 m resolution. The database contains classified soil maps based on WRB and USDA classification respectively. It also offers the soil texture, including the content of sand, silt, and clay in the soil in 7 depths (0, 5 cm, 15 cm, 30 cm, 60 cm, 100 cm, 200 cm).

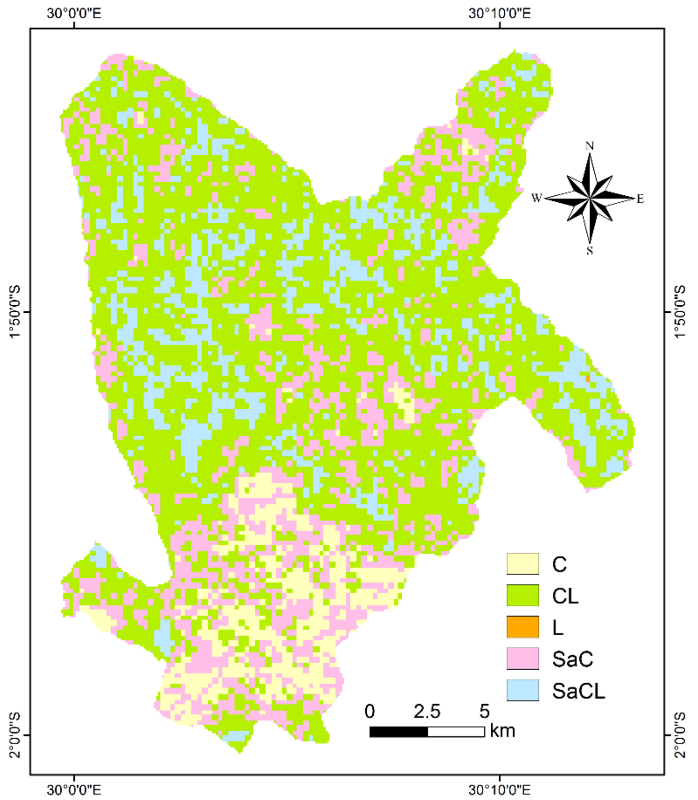

Figure 3.6 Soil class map based on Soilgrids database.

Soil properties serve for the simulation of the infiltration process. The maps with the content of sand and clay were calculated by averaging the content of sand and clay in 7 depths separately. The average content of clay and sand up to 200 cm ranges from 26% to 47% and from 30% to 54% respectively. The soil was classified according to the content of sand and clay in it through Soil Water Characteristics Program. The soil in this area includes five texture classes: clay (C), clay loam (CL), loam (L), sandy clay (SaC), and sandy clay loam (SaCL). The soil class map after classification is presented in Figure 3.6. The soil in the urban area mainly consists of C and SaC, and the rest mainly consist of CL, SaC, and SaCL. L only occupies a minimal proportion and hardly visible from the map.

Table 3.2 Hydraulic parameters of soil

Parameter	Ksat	Porosity	Suction
Unit	mm/h	-	cm
L	3.4	0.463	8.89
SaCL	1.5	0.398	21.85
CL	1	0.464	20.88
C	0.3	0.475	31.63
SaC	0.6	0.43	23.9

Saxton & Rawls (2006) and Jetten & van den Bout (2017) provided tabulated relation between soil texture and soil hydraulic properties based on laboratory experiments and regression methods. The soil properties, including saturated hydraulic conductivity (Ksat), suction at the wetting front, and porosity were applied. It is worth mentioning that according to the literature, Ksat is very low for all types of soil in the study area. The low values result in low infiltration rates thus infiltration excess overland flow can relatively quickly be generated by the model. The infiltration in the soil on the land surface and the seepage in the channel is simulated separately. On account of scarce information about the soil in the channel, no seepage is included in the model. The hydraulic properties of soil used in this study are shown in Table 3.2.

3.3. CMORPH Bias Correction

Satellite products might generate large errors in detecting precipitation, including random errors and systematic errors. The systematic errors (biases) of rainfall estimates from CMORPH require bias correction based on the rainfall data from rain gauges. The basic procedure of bias correction is to multiply SREs by the bias factor to result in a new and more accurate set of satellite rainfall estimates for use in modelling. Three bias correction schemes by Habib et al. (2014) are selected for this study: Time Space Variable (TSV), Time Variable (TV), and Time and Space Fixed (TSF). The equations are:

Time Space Variable:

$$BF_{TSV} = \frac{\sum_{t=d}^{t=d-l} G(i,t)}{\sum_{t=d}^{t=d-l} S(i,t)}$$

where i is the rain gauge number, t is the day number, and l is the length of a time window (days) for bias calculation. Different lengths of time window can be compared and applied. G and S represent the accumulative rainfall values of each gauge and its corresponding CMORPH pixel during the time window respectively. The bias factor is variable with respect to gauges and dates.

Time Variable:

$$BF_{TV} = \frac{\sum_{t=d}^{t=d-l} \sum_{i=1}^{i=n} G(i,t)}{\sum_{t=d}^{t=d-l} \sum_{i=1}^{i=n} S(i,t)}$$

where n in the numerator is the total number of rain gauges within the entire domain of the study area, in this study 2. G and S represent the accumulative weighted average values of all gauges and the average values of CMORPH during the time window respectively. The bias factor is still variable with respect to dates but lumped in spatial.

Time and Space Fixed:

$$BF_{TSF} = \frac{\sum_{t=1}^{t=T} \sum_{i=1}^{i=n} G(i,t)}{\sum_{t=1}^{t=T} \sum_{i=1}^{i=n} S(i,t)}$$

where T is the full duration of the time study period, in this study 2. G and S represents the accumulative weighted average values of all gauges and the average values of CMORPH during the simulation period respectively. The bias factor is lumped both in temporal and spatial context. (description modified after Habib et al. (2014))

Since the gauge rainfall data is in a daily interval which is different from CMORPH, half-hourly estimates of CMORPH rainfall data were accumulated to match the temporal resolution of gauge rainfall. When bias factors of each gauge were computed, rainfall estimates in each gauge were compared to the CMORPH pixel values where it is located. It is noted that two gauges (Gitega and Kigali_area) fall into the same CMORPH pixel. When the bias factors of the entire study area were computed, the weighted average estimates were compared to the average CMORPH estimates in the area.

3.4. Channel Network

3.4.1. Dimensions

A channel network is necessary to be added to a DEM map in flood modelling. The area of study is in the Nyabugogo commercial hub where the Nyabugogo river flows through. Besides, three tributaries contribute to flow in the main river, so inflow from connected sub-catchments have to be taken into account. The collected base map contains a map of drainage system including main Nyabugogo river and several tributaries. The locations of the channels were defined using the drainage system map. The DEM map of the channel was extracted from the SRTM DEM map. A description of the exact procedure is denied here and reference is made to PCRaster software (Pcraster Team, 2011)

In LISEM, the width of a channel can be set smaller than a grid size of the DEM. The channel is assumed to cross the centre of a grid cell, while the elevation of the river bank is set to be the elevation of the DEM grid cell. The cross-sections are assumed to be trapeziums or rectangles, and the dimension of a channel is determined by the width and depth of the channel, and the side angle of the river bank.

The dimension of the channel is a significant factor as it determines the channel's capability in storing and transporting water thus directly affecting inundation and flooding events. Due to lack of field measurements, the width of the channel was achieved by measuring the channel width using the available orthophoto for this study. The depth of the channel was derived from the field measurements of the river. The average value of width and depth along the river flowing through the city are 9.16 m and 2.99 m respectively that served parameterization of the channels. Cross-sections are assumed to be rectangles, so the angle of channel side was set to 0. In order to create a gradual changing channel dimensions and avoid errors resulting from rigorous changes of cross-section shapes, the dimension was set the same along the channel using the average measured values. Due to the absence of measurements in the upstream part of the main river and the tributaries, the average dimensions of the river section through the city were applied to the entire channel network. In reality, often the width of a channel typically keeps increasing from upstream to downstream, and dimensions of tributaries are usually smaller than those of the main river. By lack of data narrowing or widening of channels had to be ignored in this study. As a consequence, a major simplification was made in representing the dimensions of the channel, which would have significant effects on the results.

3.4.2. Strahler Stream Order

It is common knowledge that the distribution and density of channels affect results of modelling since channel density affects catchment response times by routing effects. In LISEM a Strahler stream ordering (Strahler, 1952) was applied to determine the channel drainage system with specified density of the channel network. PCRaster software (Pcraster Team, 2011) was used to identify respective stream orders. The order index of the main river is 7, the indices of the tributaries attached to it are 6, and the indices of the streams connected to these tributaries are 5.

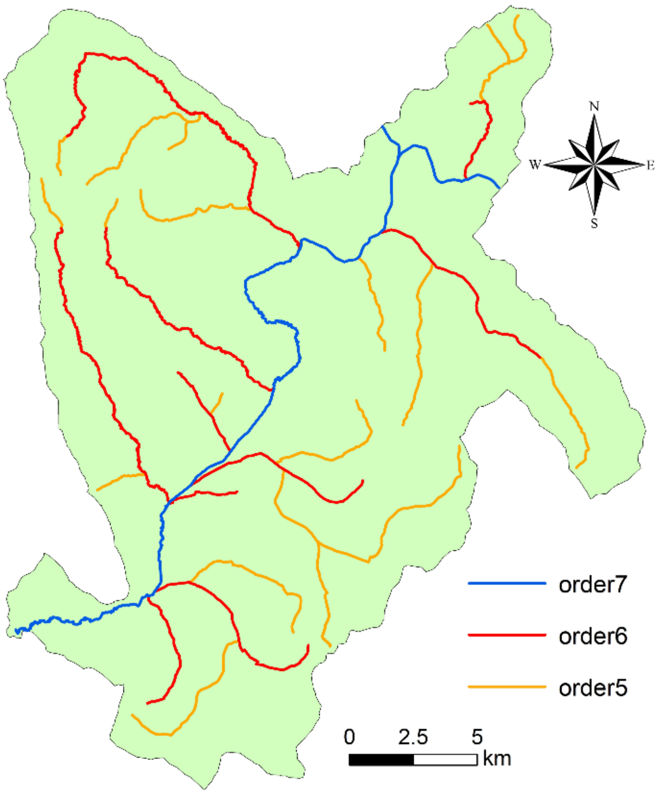

Figure 3.7 Three channel networks selected from the base map database with Strahler order indices from 5 to 7.

For this study three channel networks were defined: with highest stream order of 7, 6, and 5, respectively. All three networks are connected to the branches in the sub-catchment out of the area that served model boundary outflow. The three networks were tested, and one of them was selected in developing the model based on the results. To evaluate the effect of the channel network density on runoff, the model was run with, initial soil moisture content was 0.8 of porosity value of the soil in Table 3.2 and the soil depth was 20 cm. By applying a shallow soil layer and a high initial soil moisture content, the amount of infiltration was limited to 18 mm and caused a raise in the ratio between runoff and rainfall. All other parameters were fixed and had assigned values obtained from literature. The distribution of the channels with increasing density (i.e., lower order) are shown in Figure 3.7.

3.5. Sensitivity Analyses

Sensitivity analyses were performed to indicate how the results, particularly the discharge, change with respect to the model parameters. The main purpose of the sensitivity analyses on parameters is to determine which parameters are more efficient to calibrate a model. CMORPH rainfall data after bias correction during Event 1 and the characteristics of Nyabugogo catchment were applied.

By the LISEM structure, runoff production by interflow and/or subsurface flow is not included and thus only runoff produced by infiltration excess overland flow contribute to surface runoff and flooding. When assuming that seepage at the bottom of a soil is not possible in a model (i.e. an impermeable bottom is considered) water will be stored in a cell that possible could become saturated by infiltration. Therefore, the depth of subsurface soil layer which affects infiltration is a significant factor in LISEM. A shallow soil layer is likely to become fully saturated when a rainstorm occurs, while a deeper one is capable of storing more water and thus less runoff will be generated. However, the information of soil depth has to be achieved from in-situ measurement which is not possible in this study. Hence, different soil depths (10, 15, 20, 30, 50, 100, and 150 cm) were tested separately. The initial soil moisture content was assumed 0.7 of porosity, which is a moderate value. The porosity values are listed in Table 3.2.

Five parameters are involved in the equations computing hydrological processes in LISEM, including Manning's n of slope (surface) and channel, Ksat of slope and channel, and initial soil moisture content. Due to the uncertainty in data on land surface properties and on soil data, these parameters have to be adjusted to represent catchment characteristics better. They can be set as a ratio to the original values, which multiplies the value of every pixel in the original map at the same time. Seepage from the channel was not included in this study, so Ksat of the channel bottom was not activated resulting in a no-flow condition. Manning's n of the land surface and channel respectively, and Ksat of the soil was increasing or decreasing sequentially by 20%, 40%, and 60% while other parameters and settings remained unchanged. Different initial soil moisture contents (0.5 to 0.9 of porosity) were tested. According to the analyses above, which is stated in Section 4.3.1 and 4.3.2, the second channel network was selected, and the soil depth was set as 20 cm.

3.6. Model Calibration

The observation interval of the historically observed discharge is daily that for this study area is inadequate for flood modelling purposes. As an alternative, the target of model calibration was to fit the main river discharge from LISEM simulation to results obtained in Manyifika (2015) that was based on HEC-HMS simulation.

The simulation period for each event was two days. Before simulation, the channel flow domain was initialized for the day that preceded the rainfall events. The target base flow was adopted from Manyifika (2015). The LISEM outlet discharge was reported every 1 min, which is the same as the computation time step. Following the sensitivity analyses results, channel networks and depths of soil layer were fixed. The first target of calibration was to fit the volume of total discharge during the simulation period, as it indicates the water balance of the model. In flooding events, inundation is usually generated when the discharge approaches a high flow event value, in this study highest peak flow event values for each event are considered. The second target was to fit the peak flow volumes for each rainstorm. When initial soil moisture content increases, both total discharge and highest discharge increases. In this case, when Ksat increases in a limited range, highest discharge still increases, while total discharge decreases. Manning's n of the land surface and the channel were not adjusted as these were not very sensitive parameters. Ksat of the soil during four events was set as the same value to represent the soil properties in this area. Since LISEM was developed to simulate a single event, initial soil moisture was set different in each event.

An objective function, Relative Volumetric Error (RVE) (Haile, Tefera, & Rientjes 2016), was selected to assess the model performance. Apart from it, the error in the volume of peak discharge, Δ, was also used in the assessment. Both are used to assess if LISEM is able to simulate the peak volume and peak discharge respectively. The equations are:

Relative Volumetric Error:

$$RVE = \frac{\sum_{i=1}^{n}(Q_{obs,i} - Q_{sim,i})}{\sum_{i=1}^{n} Q_{obs,i}} * 100\%$$

where $Q_{obs,i}$ is HEC-HMS simulation, $Q_{sim,i}$ is LISEM simulation, and n is the number of simulation steps. The total volume of discharge (m^3) during the simulation period was calculated from reported discharge in every time step (m^3/s).

Difference Δ:

$$\Delta = \frac{Q_{sim,peak} - Q_{obs,peak}}{Q_{obs,peak}} * 100\%$$

where $Q_{obs,peak}$ is peak discharge of HEC-HMS simulation, and $Q_{sim,peak}$ is peak discharge of LISEM simulation. Two peaks and difference Δ in every event were computed and compared separately.

The optimum values of RVE and difference Δ are both 0, which means a small difference in the magnitude of total and peak discharge. Visual inspection was also required in fitting the hydrograph.

3.7. Flood Forecasting

The model was calibrated to fit the main river discharge from LISEM simulation to results obtained in Manyifika (2015) based on HEC-HMS simulation, and optimum model parameters were achieved after calibration. Flood forecasting procedure was then performed to evaluate if LISEM is capable of simulating the discharge with ECMWF rainfall forecasts serving as the meteorological inputs of the model. In the flood forecasting procedure, the simulation period was set at two days (48 hr).

The principle is explained in Figure 3.8. ECMWF forecasts were released every 12 hr, so the forecasting was operated with lead times from 12 to 48 hr. When the lead times changed, different combinations of rainfall inputs (ECMWF and CMORPH) were used in the model, while the model parameters and initial conditions remained the same as set during calibration. The temporal resolution of ECMWF and CMORPH inputs should match to make the results of forecasting comparable. Since the temporal resolution of ECMWF forecasts is 6 hr, also CMORPH estimates were defined for every 6 hr.

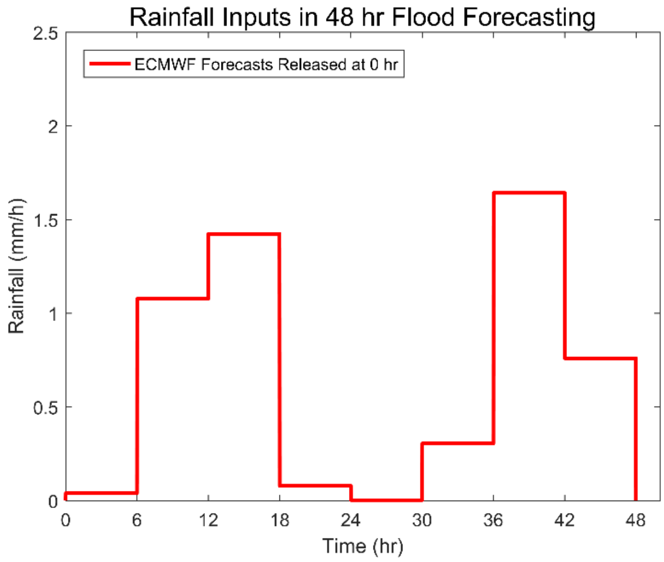

When the flood forecasting with 48 hr lead times were operated, ECMWF rainfall forecasts released at 0 hr served as rainfall inputs and covered the entire 48 hr.

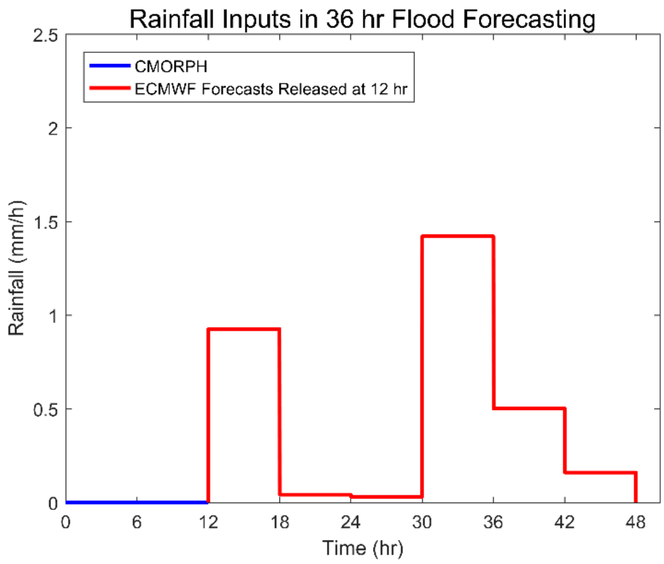

When the lead times became 36 hr, the first 12 hr was treated as past time, and rainfall inputs in the first 12 hr were replaced by bias-corrected CMORPH rainfall estimates. ECMWF forecasts released at 12 hr were used in the remaining 36 hr.

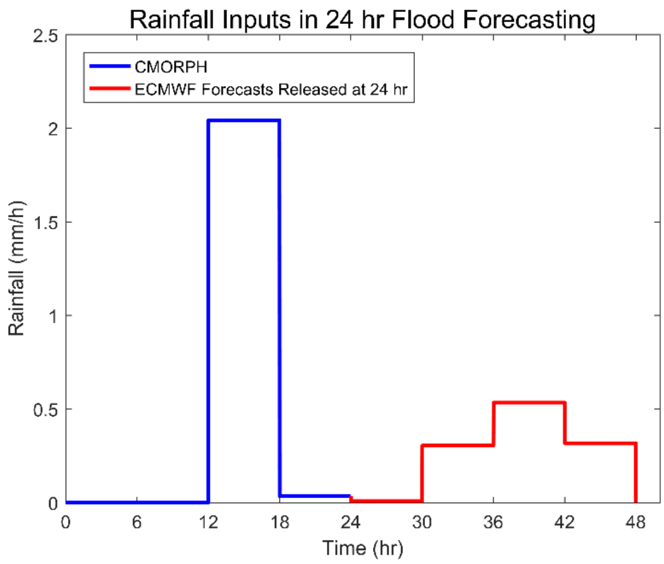

When the lead times were 24 hr, CMORPH estimates were used in the first 24 hr, and ECMWF forecasts released at 24 hr were used in the remaining 24 hr.

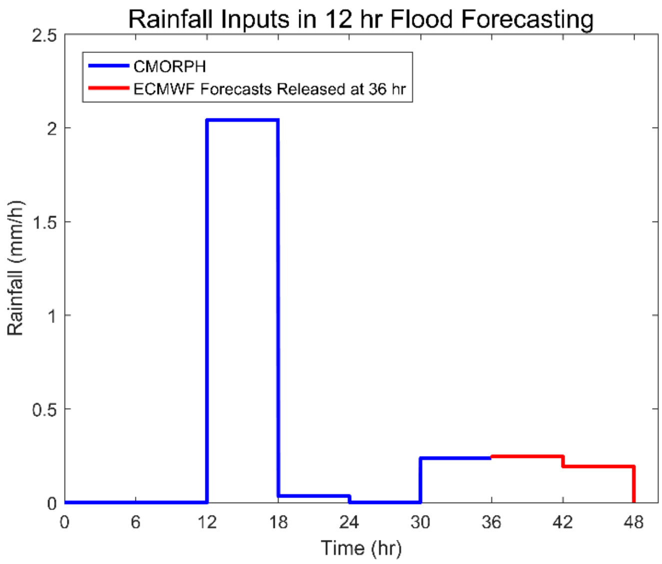

When the lead times were 12 hr, CMORPH estimates were used in the first 36 hr, which was treated as past time. ECMWF forecasts released at 36 hr were used in the last 12 hr.

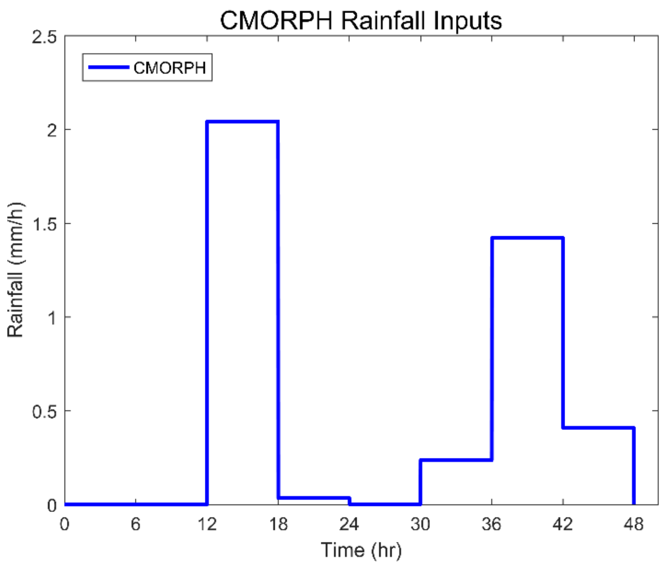

CMORPH rainfall estimates were treated as actual observation, so simulation results when CMORPH estimates covered the entire 48 hr reference to when the forecasted ECMWF rainfall inputs were used.

Figure 3.8 Procedure and rainfall inputs of flood forecasting using ECMWF precipitation forecasts and corrected CMORPH estimates with lead times from 12 to 48 hr.

The forecasting procedure can be applied to all the four flooding events. However, the biggest rainstorm in Event 2 occurred at the midnight of the second day, and the peak discharge resulting from it appeared on the third day of the event. Therefore, it was considered not meaningful to perform a forecasting procedure with lead times of two days as it could not capture the peak discharge. In addition, the rainfall estimates of CMORPH pronouncedly deviate from in-situ measurements in Event 2. It might lead to unreliable simulated results and thus not suitable to use in the evaluation of the performance of the forecasts. Thus, the forecasting procedure was operated in Event 1, 3, and 4.

Similar to calibration, quantitative assessment served to assess the performance of forecasting. Regarding scores or measures to indicate the quality of forecasts, Jolliffe & Stephenson (2003) provided a number of scores suitable for different kinds of forecasts. For instance, continuous ranked probability score (CRPS) is widely used in evaluating probabilistic forecasts, and anomaly correlation coefficient (ACC) can be used in evaluating forecasts in spatial fields. However, due to the very small number of forecasts in this study, basic scores are the most appropriate. Root Mean Square Error (RMSE) was selected to reflect the deviation between results achieved from ECMWF forecasts and CMOPRH estimates in each time step. The equation to compute RMSE is:

$$RMSE = \sqrt{\frac{\sum_{i=1}^{n}(Q_{obs,i} - Q_{sim,i})^2}{n}}$$

where $Q_{obs,i}$ is simulation based on CMORPH estimates, $Q_{sim,i}$ is simulation based on ECMWF rainfall forecasts, and n is the number of simulation steps. The unit of RMSE in this case is m3/s and the best value of it is 0.

4. RESULTS AND DISCUSSIONS

4.1. CMORPH Rainfall Estimates

4.1.1. Bias Correction

Figure 4.1 indicates for each flood event the daily average rain values for the study area from in-situ measurements and raw CMORPH estimates for a time period that covers 15 days before a flood event and 2 days after the onset of the event. CMOPRH succeeds to capture the highest rain values on day -5 and 1, two days before and during Event 1. In Event 3 and 4, CMORPH and in-situ measurements have the same outstanding dates, including day -7, -4 and -1 in Event 3, and day -5, -2 and 0 in Event 4. However, the magnitude of rainfall detected from CMORPH is not so accurate. Among these four events, the performance of CMORPH is the worst in Event 2. It provides miss detection when no heavy rainfall occurs and fails to capture all the heavy rainfall, especially on day 1 during the event, when in-situ measurements detect a rainstorm and a flood event is recorded.

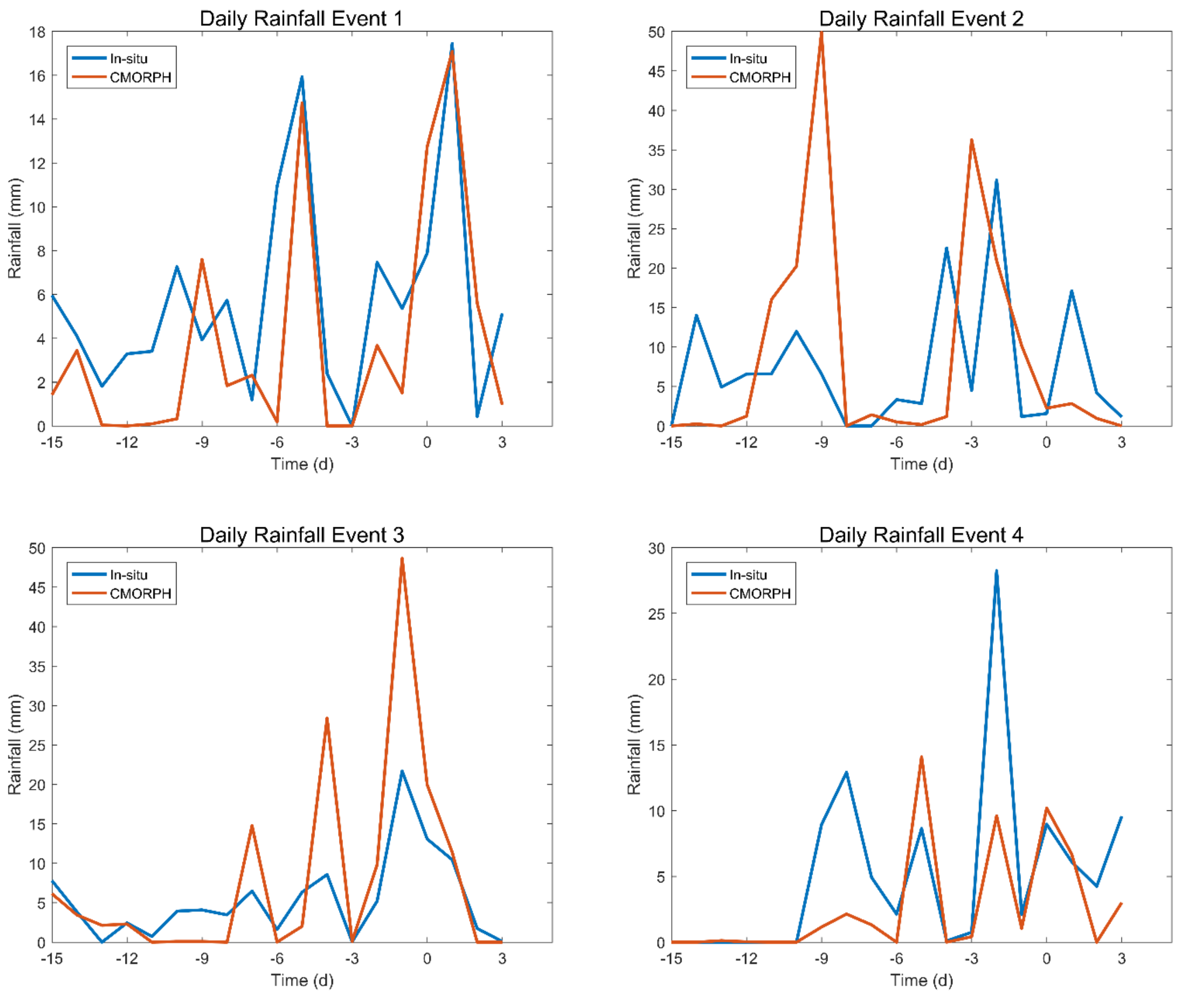

Figure 4.1 Daily average rain values for the study area from in-situ measurements and raw CMORPH estimates for a time period that covers 15 days before a flood event and 2 days after the onset of the event

Table 4.1 listed the bias factors of CMORPH using Time Variable method with length of time window from 2 to 7 days for the eight days of the four selected events as well as the mean values and the standard deviation of them. The standard deviation of all dates is in a low range in Event 1, 3, and 4, which shows that errors of CMORPH in theses dates mostly results from systematic errors. Therefore, the selection of the length of time window is likely not to have major effect on the flooding results in these three events.

Table 4.1 Bias factors of CMORPH using Time Variable method with the length of time window from 2 to 7 days.

Time window (d)	7	6	5	4	3	2	Mean	Std.
Event1 day1	1.13	1.16	1.09	1.09	0.98	0.85	1.05	0.12
Event1 day2	1.01	0.95	0.95	0.84	0.73	0.79	0.88	0.11
Event2 day1	1.10	1.06	0.77	1.41	1.30	3.68	1.55	1.07
Event2 day2	1.10	0.81	1.49	1.48	3.79	5.63	2.38	1.91
Event3 day1	0.54	0.50	0.56	0.56	0.57	0.75	0.58	0.09
Event3 day2	0.51	0.58	0.58	0.59	0.81	1.07	0.69	0.21
Event4 day1	1.31	1.66	1.65	1.65	0.96	0.89	1.35	0.36
Event4 day2	1.81	1.80	1.80	1.20	1.14	1.55	1.55	0.31

Concerning Event 2, it is shown in Figure 4.1 that the most variance between CMORPH estimates and in-situ observation is on the second day, on which rain gauges detected heavy rainfall but CMORPH did not. In fact, the highest discharge peak of this catchment from 2011 to 2013 appears around the dates of Event 2, which proves that the estimates from in-situ observation is more accurate. It seems that CMORPH misses a large quantity of rainfall detected by the rain gauges on the second day of Event 2 while its estimates on the first day match in-situ measurements well. Therefore, the target of bias correction for Event2 is to largely raise the rain values on the second day and maintain the values on the first day at a similar range. A three-day time window is then the most appropriate for Event 2. Therefore, the time window in calculating bias factors was set at three days although a longer window, for instance seven days, is more commonly applied as shown in (Habib et al., 2014). The bias factor of each day was computed separately, and it was in the middle of the time window.

Table 4.2 Bias factors of CMORPH using three methods with length of time window as three days.

Method	Gitega	Kigali_aero	Rubungo	Cyinzuzi	TV	TSF
Event1 day1	1.04	0.84	0.72	1.19	0.98	0.85
Event1 day2	0.97	0.77	0.62	0.68	0.73	0.85
Event2 day1	2.41	0.64	1.40	0.00	1.30	3.68
Event2 day2	6.09	1.22	3.64	2.09	3.79	3.68
Event3 day1	1.17	0.27	0.62	0.27	0.57	0.75
Event3 day2	1.08	0.25	1.05	1.01	0.81	0.75
Event4 day1	0.84	1.56	0.09	1.47	0.96	0.89
Event4 day2	0.89	1.75	1.12	1.26	1.14	0.89
Mean	1.81	0.91	1.16	1.00	1.28	1.54

Time Space Variable, Time Variable and Time Space Fixed methods of bias correction were used to compute bias factors of CMORPH in each rain gauge and the whole study area. The factors of eight days in four events were computed using a three-day time window and are shown in Table 4.2. Bias factors in each gauge were obtained using the TSV method, and the TSF method considers an event as an ensemble and provides the same factor for two days in it. Bias factors on two days of Event 2 are very large (3.86) and are outliers among the eight days and provide enormous values, which is consistent to Table 4.1. Except them, most factors are around 1 provide moderate values. In general, CMORPH failed to capture a significant number of rainfall values during Event 2 but did not underestimate rainfall values significantly in the rest days (Figure 4.1).

Except Event 2, the feature of these factors is apparent. Among the four rain gauges, the performance of CMORPH is the best in Gitega and much better than the others. The other gauges have factors that vary substantially. Due to the limitation of sample numbers, no clear relation between rain gauges and the magnitude of bias factors is found. Concerning the entire study area, factors computed using spatially lumped methods (TV and TSF) all are around 1. It can be concluded that spatially lumped methods tend to provide more continuous values compared to the factors in a single rain gauge. The overall performance of CMOPRH in this area is considered acceptable.

The density of rain gauges in the study area is relatively low, in which only four gauges are located in the area that is of size 454 km^2. To reduce the effects of occasional extreme values in a single gauge, using one factor for the entire area seems to be more proper. As the variance between the factors in two days within an event should not be neglected, the Time Variable method was selected to correct CMORPH estimates for flood simulation.

4.1.2. Rainfall Patterns

Figure 4.2 shows the rainfall time series during the events of CMORPH raw data and after bias correction using the scheme explained before. The period of Event 2 was extended by one day as a rainstorm occurs at the midnight of the second day, and it is the same in flood simulation. These lines represent the average values in the whole study area, therefore the spatially distributed patterns are not indicated. All the four events have two storms, and there is no rainfall in the rest of time in the two days. According to the graphs of raw CMORPH, the first storm usually starts from 10:00 to 14:00 on the first day and lasts for about 6 hr, and the second one usually starts from 8:00 to 12:00 on the second day and lasts for about 12 hr. It seems that the rainstorms leading to flooding in this area share some similar feature and heavy rainfall usually starts at about noon. The first storm is more continuous and has much higher maximum intensity, while the second one has lower intensity and a longer duration, which usually lasts to the night.

After bias correction, all the rainfall with highest intensity is reduced except in Event 2, in which raw CMORPH provides very slight rainfall. According to corrected CMORPH, the highest intensity of the second storm in Event 2 and 3 becomes higher than that of the first one. Among the four events, the maximum intensity and accumulative amounts of rainfall are higher in Event 1 and 3 and lower in Event 2 and 4, which might lead to a difference in the outlet discharge and the inundated area.

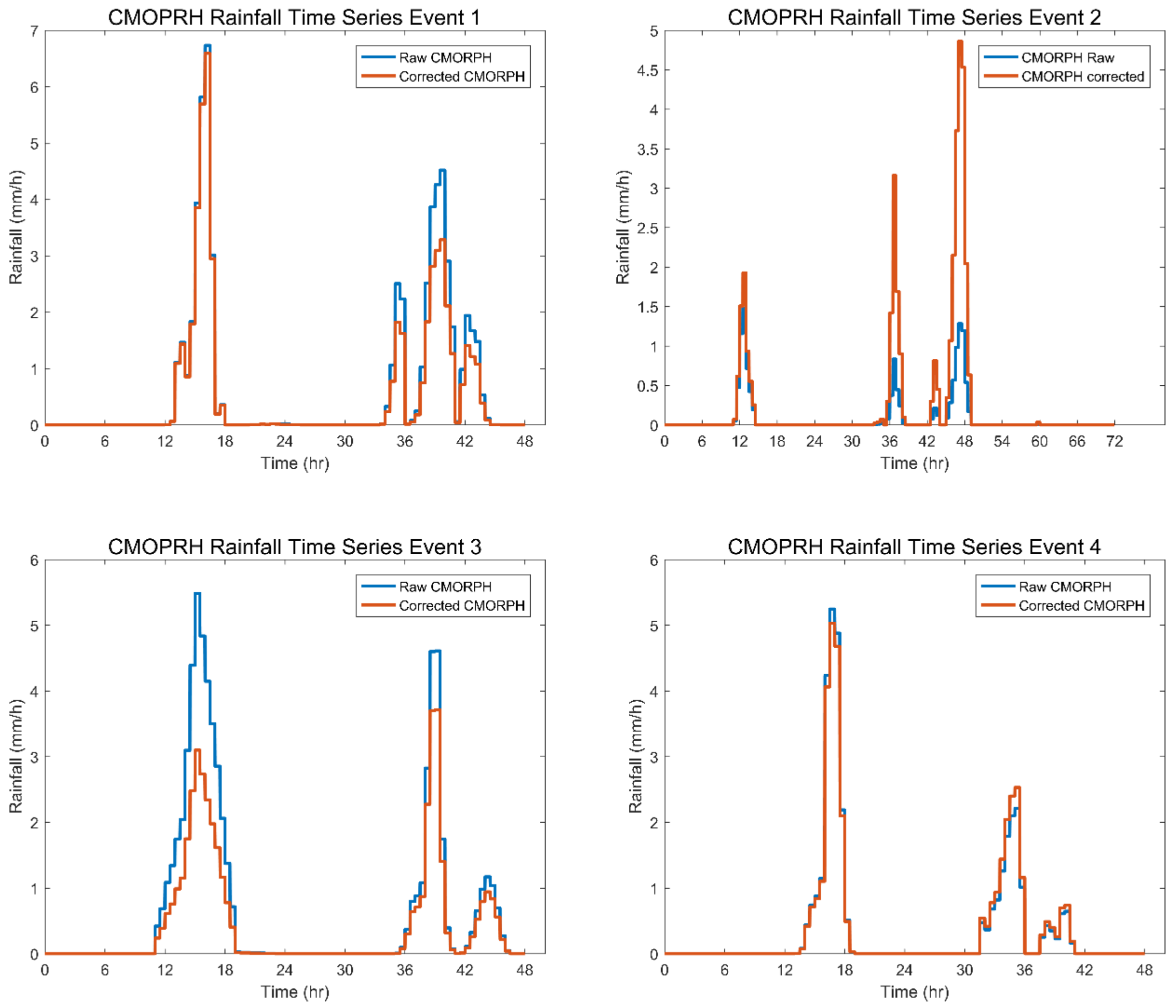

Figure 4.2 Rainfall time series from raw and corrected CMORPH estimates in two-day events. The period of Event 2 was extended by one day as a rainstorm occurs at the midnight of the second day.

Figure 4.3 illustrated the spatially distributed patterns of accumulative rainfall during the four events from CMORPH raw estimates and bias-corrected estimates. Pixels carrying the highest values, which are dark blue in the images, are more frequently observed in raw data. Most of them overlap with the boundary of the study area, which reveals that heavy rainfall also occurs in the other sub-catchments when these flooding events occur. These amounts of water from the other sub-catchments were represented using sub-catchments inflow of the model, the values of which are based on HEC-HMS simulation. After bias correction, those highest values were reduced, and the pixels with dark blue are not observed anymore. It seems that the extremely high values are reduced by means of bias correction, both in temporal and spatial aspects. Besides, the deviation among the pixels in an image decreased after bias correction. Event 2 is exceptional since raw CMORPH only detected minimal rain values and the rain values were primarily increased after bias correction.

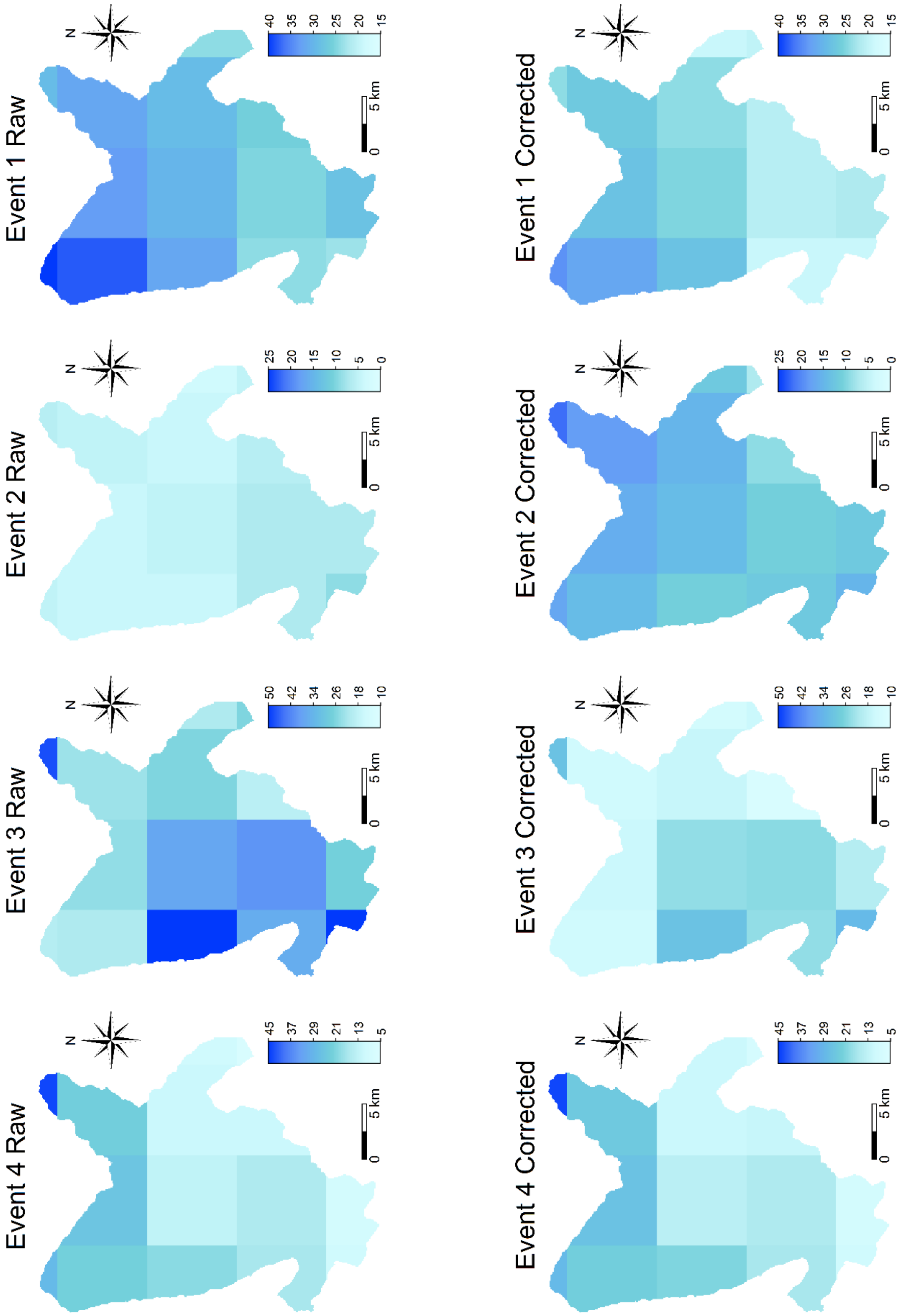

Figure 4.3 Spatially distributed patterns of accumulative rainfall in two day events in the study area from raw and corrected CMORPH estimates.

4.2. ECMWF Rainfall Forecasts

The total rainfall values for two-day events from in-situ measurements and ECMWF forecasts with lead times from 2 to 7 days are compared in Figure 4.4 (a). The different values in one line represent the updated forecast estimates for decreasing forecast lead times from day 7 to the day in-situ data is shown. In the graphical representation on updated forecast, lead times are shown backward in time to allow direct comparison with in-situ observations at respective days. Considering in-situ measurements as the most representative estimates, the performance of a forecast can be reflected by the variance between it and in-situ measurements. There is no definite relation between lead times and the magnitude of forecasts or a regular trend of these forecasts. Besides, the accuracy of forecasts does not reduce remarkably as lead times become longer in these events. Regarding the difference among the forecasts with changing lead times, Event 1 and 2 have more continuous forecasts and lower standard deviation (2.57 mm and 3.44 mm) among these values, while Event 3 and 4 have higher (9.47 mm and 6.98 mm).

A comparison between accumulated total rainfall estimates from ECMWF forecasts with two day lead times to, raw and corrected CMORPH, and in-situ measurements are shown in Figure 4.4 (b). Histograms show that raw CMORPH overestimates rainfall compared to in-situ data except for Event 2. When raw CMOPRH estimates largely deviate from in-situ data, bias correction is able to reduce the deviation, which is also observed in Figure 4.3. After correction, the difference between CMORPH and in-situ measurements is in an acceptable range. In Event 2 and 3, ECMWF forecasts match the in-situ measurements very well.

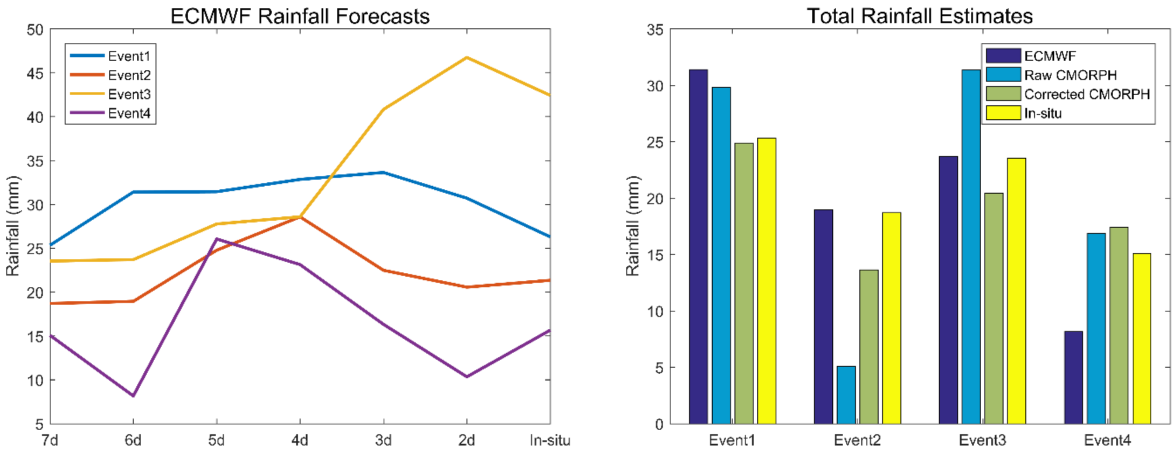

Figure 4.4 (a) ECMWF rainfall forecasts for two-day events with lead times from 2 to 7 days and in-situ measurements. The different values in one line represent the estimates on the same dates with different lead times. (b) Total rainfall estimates for two-day events from various sources.

Figure 4.5 shows the spatial patterns of ECMWF precipitation forecasts with 48 hr lead times. These images represent accumulative rainfall, the periods and the scales of which are the same as Figure 4.3. Apparently, the spatial resolution is much coarser than that of CMOPRH, which is a drawback of this product. The study area is covered by only four pixels, and none of them falls completely in it. Besides, the values from the four pixels in an image are mostly close to each other. Compared to corrected CMORPH estimates, ECMWF 48 hr forecasts provide more rainfall in Event 1 and 2, similar rainfall in

Event 3, and much less rainfall in Event 4. It is reflected in Figure 4.4 (b) as well and results in discharge disparity in the flood forecasting procedure.

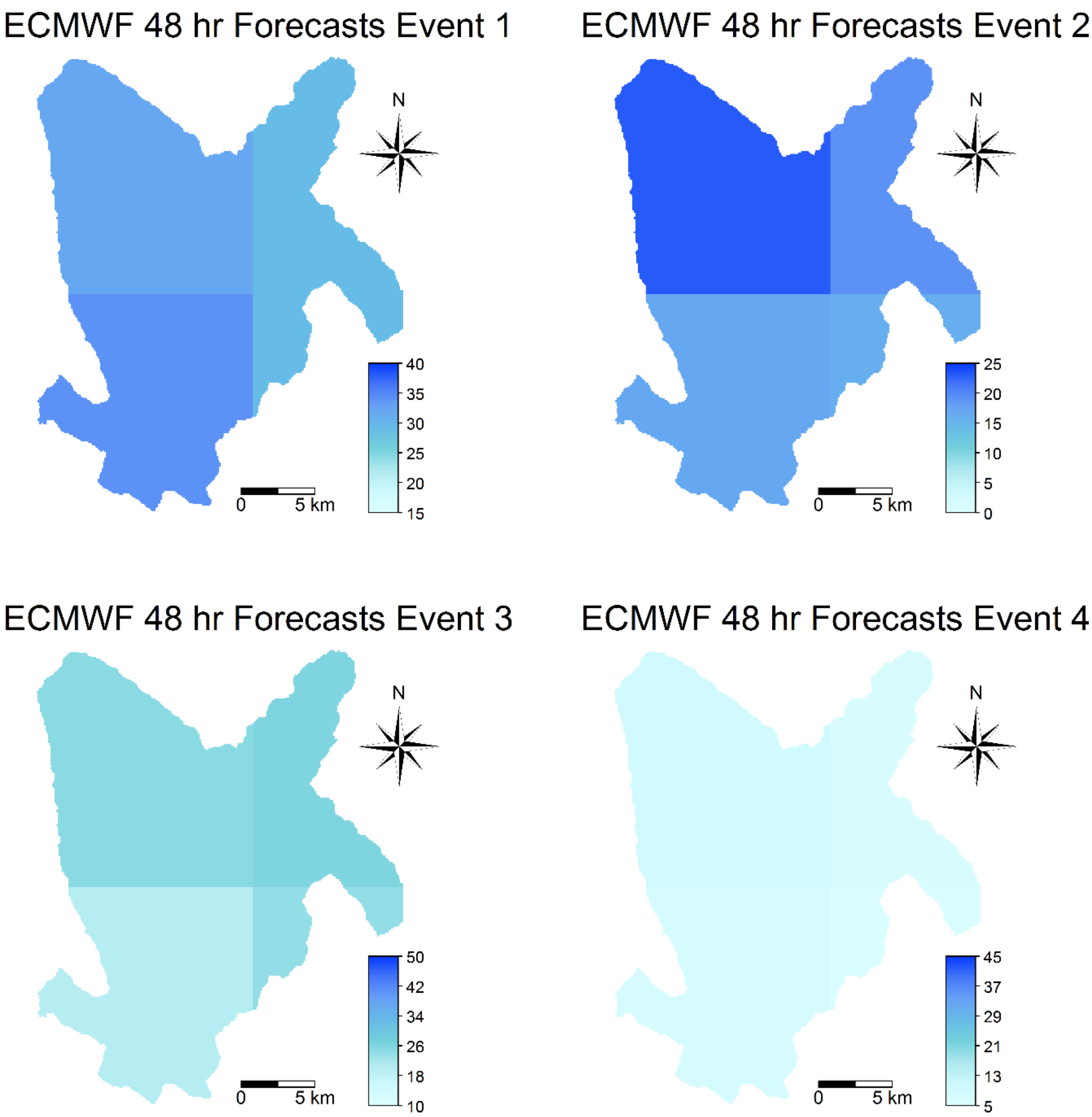

Figure 4.5 Spatial patterns of ECMWF precipitation forecasts with 48 hr lead times. The values represent accumulative rainfall during a two-day event.

4.3. Model Development

4.3.1. Strahler Stream Order

Three channel networks based on Strahler stream order are tested for flood simulation in this study. The total lengths of the three networks are 46, 134, and 215 km respectively. The length increases noticeably when more streams with lower order are added to the network. The hydrographs obtained by these channel density representations are shown in Figure 4.6 (a). It can be seen that the outlet discharge increases dramatically when 6th order rivers are added to the network. The peak discharge of channel 2 is close to 4 times of channel 1. The discharge is even larger when 5th orders are combined, but the variance is not as considerable as the former though the rise in the total length is more massive.

The reason of the discharge variation is explained in Figure 4.6 (b), which indicates the proportion of outlet discharge, surface runoff (water remaining on the land surface at the end of simulation), and infiltration in three simulations. It is evident that the amount of infiltration is not affected by the density of channels. When the density rises, more water flows to the catchment outlet in the same simulation time, and less water is left on the land surface.

However, the shift in time when maximum discharge appears is somewhat surprising in a manner that the peak time delays instead of advancing as the channel density increases. Manning's Equation is applied to the surface water flow simulation, and the velocity of channel flow is normally much higher than that of overland flow. Consequently, a denser channel network can converge more water from the land surface promote it to flow faster along the channel. The change of velocity can be directly observed from the shift of peak time. Figure 4.6 (a) suggests that there is no considerable difference between the water flow velocity in channel flow and surface flow in LISEM.

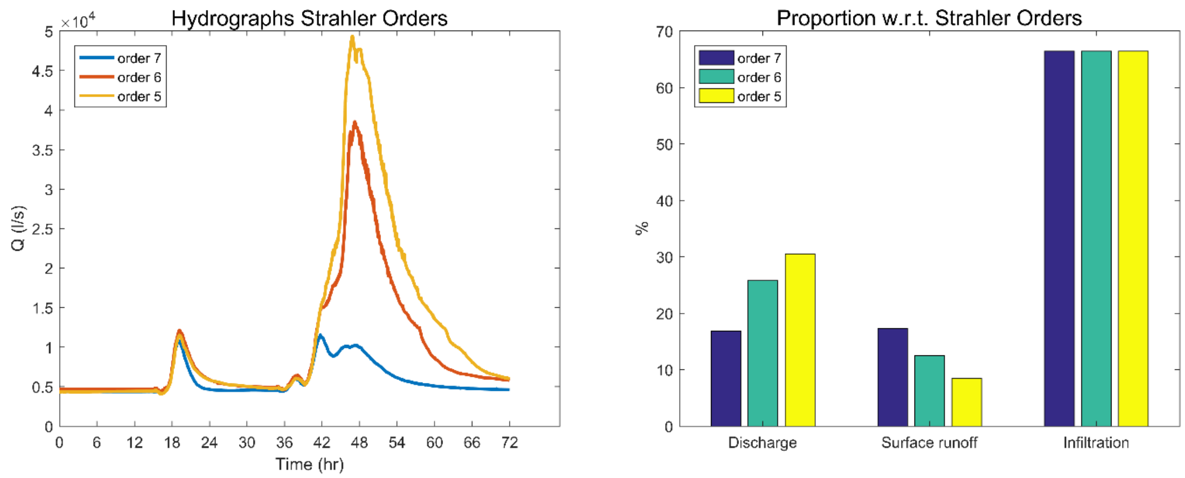

Figure 4.6 (a) Hydrographs from simulations using channels with Strahler orders from 5 to7. (b) The proportion of water processes (ratios between them and total rainfall) with respect to Strahler orders in three simulations.

A possible explanation reason is that in the principle the computation of channel flow is different from that of overland flow. In overland flow, water is possible to be stored in local depressions in the cells lower than all surrounding cells, affecting the magnitude of discharge at catchment outlet. In channel flow, however, the depressions which are lower than both the upstream and downstream cell elevations are lifted (sink-fill operation) to create a continuous channel flow. Therefore, the magnitude of outlet discharge rises with respect to a denser channel network since less water is stored in the depressions.

The maximum water depth on the land surface during the entire simulation period is an indicator of flooding extent. Depressions in a single cell and valleys can also be located at a low elevation in the local cell and much higher elevation in the surrounding cells. Figure 4.7 shows the difference in it between the simulations with three networks. Initial soil moisture was not a high value, thus there is no inundation on most of the cells. It can be seen that there is no big difference in most areas, but distinct change in some cells where new channels are added. The decrease of maximum water height in these cells is evidence that some local depressions are eliminated by defining channels. Thus, water in these cells tends to converge to the main river instead of being stored on the surface.

Most of the 6th order rivers are the main rivers in the sub-catchments where they are located in, so they have more capability in collecting surface flow. Moreover, as streams with relatively higher orders, their sizes can be approximated to be the same as the main river. The dimensions of the smaller and lower order branches are more difficult to estimate due to the absence of measurements. Thus, channel with Strahler order 6 was selected to represent rivers in the study area.

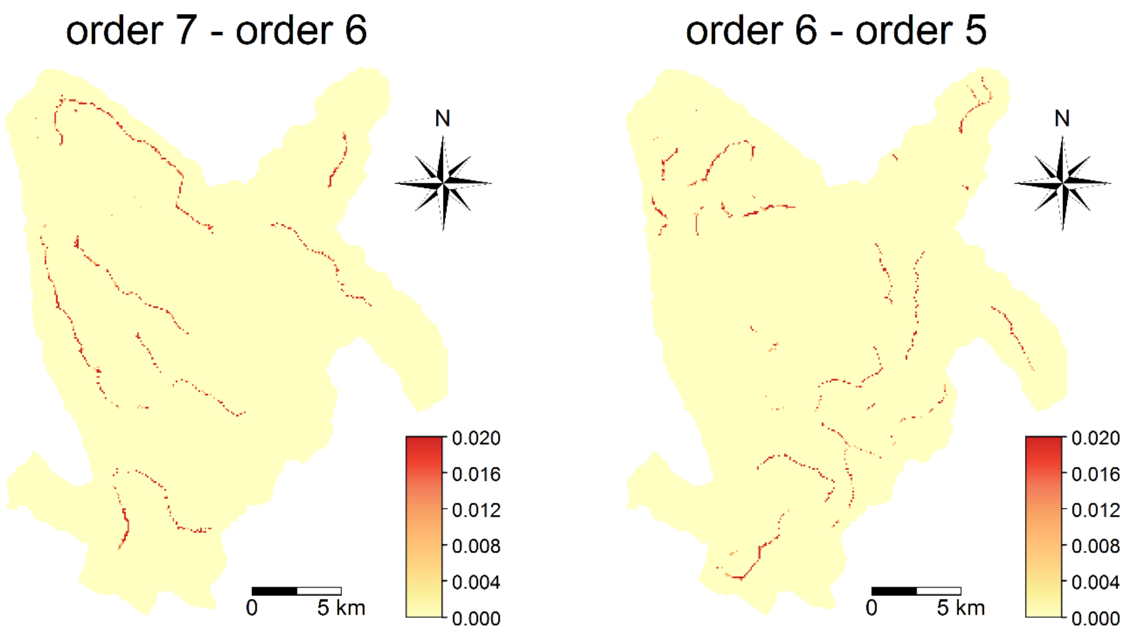

Figure 4.7 Difference in the maximum water depths during simulations between Strahler orders indices of 7 and 6, and 6 and 5 (unit: m).

4.3.2. Model Parameters

Figure 4.8 (a) shows the simulated streamflow hydrographs with depths of the soil layer from 10 to 150 cm. It is shown that only the results with 10 and 15 cm soil layer deviate from the others. The discharge is extremely sensitive to the depth when it is smaller than 20 cm. When the depth exceeds 20 cm, the value is indifferent to the results. It appears that less rainfall is stored by means of infiltration and it takes less time for water to fill in the soil layer when a shallower layer is applied. In addition, the system should have a quicker response and the peak time of discharge is expected to advance. However, it is not directly observed in the analysis of channel networks.

Figure 4.8 (b) illustrates the ratio between infiltration and rainfall with respect to the depths of the soil layer. When the depth is larger than 20 cm, the rate becomes stable and maintain at about 85%, which a very high value. As a result, very less runoff would be generated, and no flooding would occur. A shallower layer is preferable to avoid too much infiltration, but an excessively shallow layer might be problematic in calibration due to high sensitivity. A moderate value, 20 cm, was selected in this study. More runoff can be achieved by defining higher initial soil moisture.

Figure 4.9 presents the hydrographs when the model was run with different parameters, including initial soil moisture, Ksat in downward, i.e., vertical 'Z' direction across soil depth, Manning's n of the land surface, and Manning's n of the channel. The indicators of initial soil moisture (0.5 to 0.9) are relative values (ratio between absolute initial soil moisture and porosity). The graphs show that the initial soil moisture is effective on the outlet discharge only when exceeding 0.7. When the value is close to 1, which means the soil layer is almost fully saturated, the discharge rises significantly.

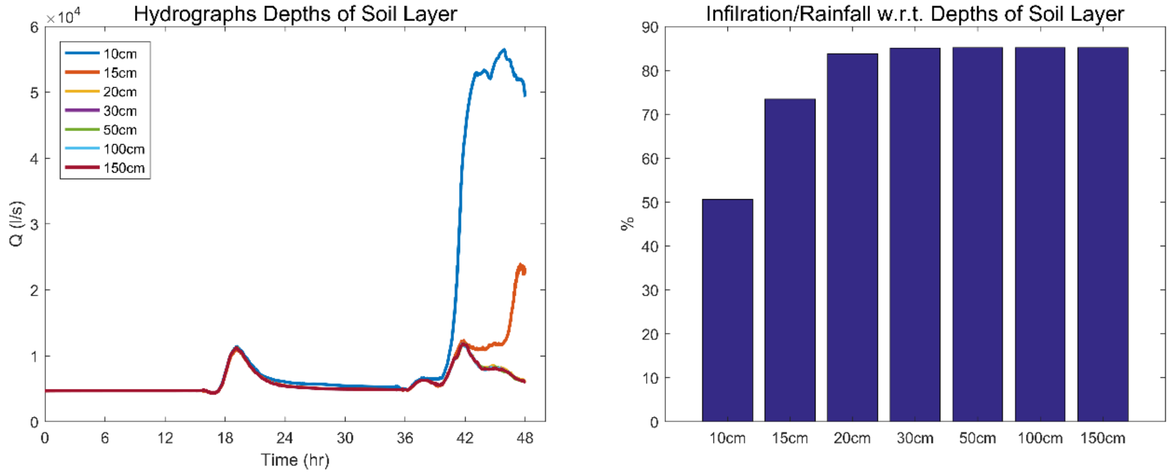

Figure 4.8 (a) Hydrographs with depths of soil layer from 10 to 150 cm. (b) The ratio between infiltration and rainfall with respect to depths of soil layer.

The indicators of Ksat, Manning's of the channel, and Manning's n of the land surface (-60% to +60%) represent the change of these parameters. For instance, +20% in the graphs of Ksat means that Ksat values in the entire area were increased by 20% from the original values in literature. The model was then run with adjusted Ksat values and the other parameters remained unchanged. Due to the relatively low original values, an increased Ksat does not make a lot of difference on the results. A decreased Ksat leads to an apparent rising of discharge by means of reducing infiltration. A changed Manning's n of land surface creates a change in magnitude and a shift in time of the discharge peak. When Manning's n of the land surface is lower, the maximum discharge is larger, and the peak time advances. However, the variance of both the maximum discharge magnitude of the shifting of peak time is minimal. The change in Manning's n of the channel sections causes almost no difference to the results. In general, the most sensitive parameter is the initial soil moisture, followed by Ksat that directly affects infiltration and thus soil water storage, while Manning's n of both the land surface and the channel are the least sensitive parameters in this case. However, the sensitive parameters are only effective to the magnitude of discharge. It seems that the peak time of discharge cannot be shifted in an efficient way by adjusting all the parameters.

Model parameters were adjusted in calibration. Manning's n of slope and channel remained the same as original values. Initial soil moisture contents in 4 events were adjusted to 83%, 82%, 85%, and 84% of porosity, which were relatively high values. As one of the most sensitive parameters, the values in four events are very close among each other. It represents the generality of these flooding events that the soil was usually almost saturated before the highest discharge peak appears. Ksat became twice of its original values, and the infiltration process was still very limiting during the events due to low original values.

However, on account of high initial soil moisture content and shallow soil layer, the soil was fully saturated at the end of the simulation period.

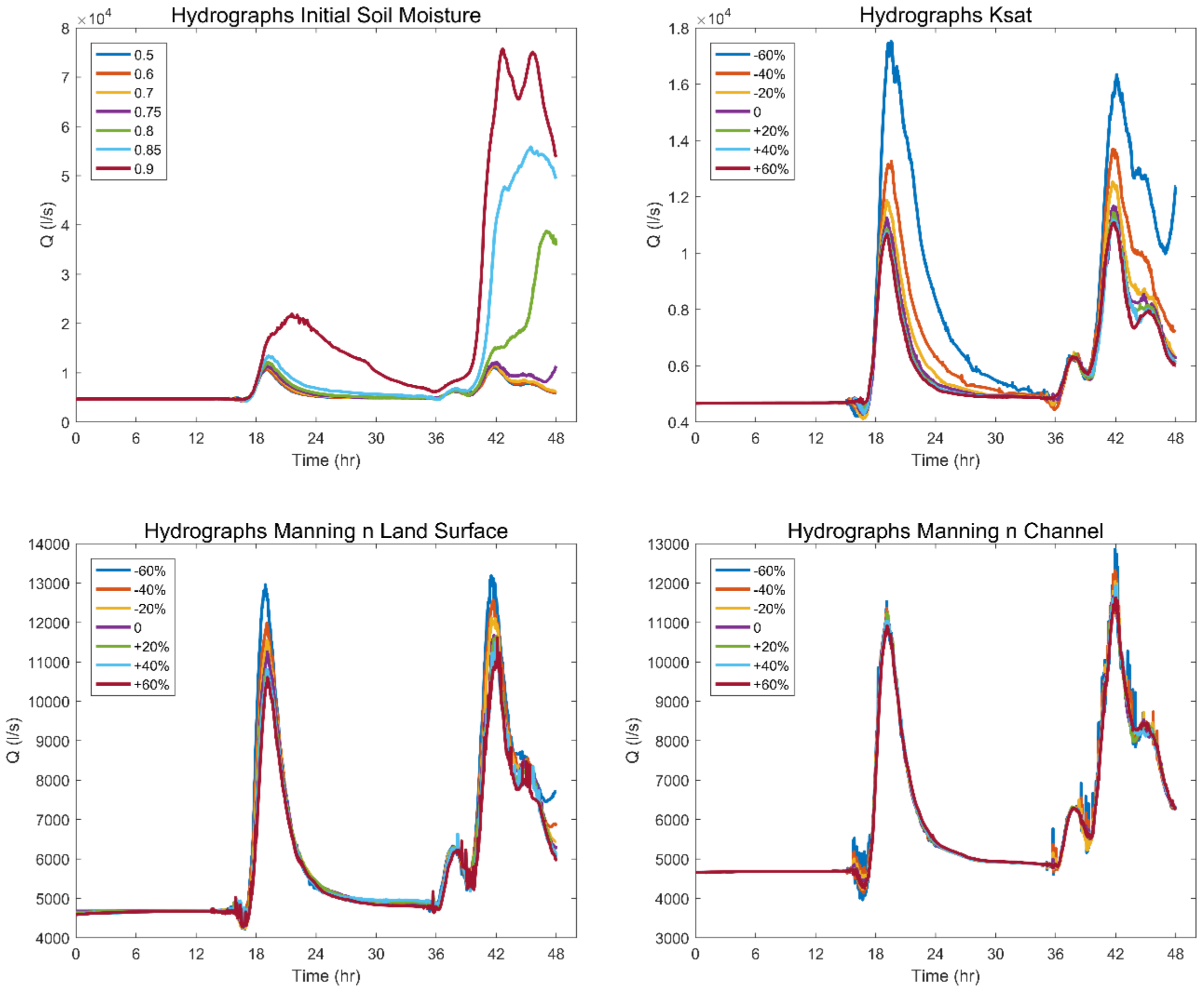

Figure 4.9 Hydrographs from simulations using changing model parameters.

4.3.3. Model Calibration

LISEM simulated discharge was calibrated to fit the discharge from HEC-HMS simulation during the two day events. The hydrographs of them are compared in Figure 4.10. The discharge is larger in Event 1 and 3 and smaller in Event 2 and 4, which has the same characteristic with CMORPH rainfall estimates. When the first storm occurs, rain water is usually infiltrated to the soil. Moreover, lateral transport of soil water to create groundwater flow is not possible in LISEM. Therefore, most water is stored in local cells and lateral discharges cannot be created unless the soil layer becomes saturated, so rainwater becomes overland flow. Among the four events, the second discharge peak is always higher than the first one, since rain intensities provided by CMORPH estimates during these events are too low to create Hortonian overland flow. In the second storm, a significant amount of rainwater is already stored in the soil layer, and new rainfall is easy to create saturation overland flow and converge to the channels be routed to the outlet. Regarding HEC-HMS, the amount of discharge is directly affected by rainfall in very short period, thus the feature is observed.

The hydrographs of LISEM have a systematic delay compared to those of HEC-HMS in all the events, both in the rising limb and the falling limb in the hydrographs. It is due to the different theories on how runoff is produced of the two models. In HEC-HMS, the rainfall-runoff relation is computed separately in every sub-catchment. Besides, it is well defined which runoff production mechanisms actually are simulated by HEC-HMS, it is noted that rainfall is lumped in spatial. The rainfall is relatively simply converted to discharge in the outlet of sub-catchment with a delay time related to the area of it. Discharge of each sub-catchment at the same time is then simply added to the total discharge. In LISEM, rainfall and catchment characteristics are spatially variable, and the direction and velocity of water flow are computed based on physical equations. The water on the surface and in channels finally converges to the catchment outlet. In terms of theory, the distribution and movement of water with respect to time can be better traced. Therefore, the peak time of discharge in LISEM is more representative.

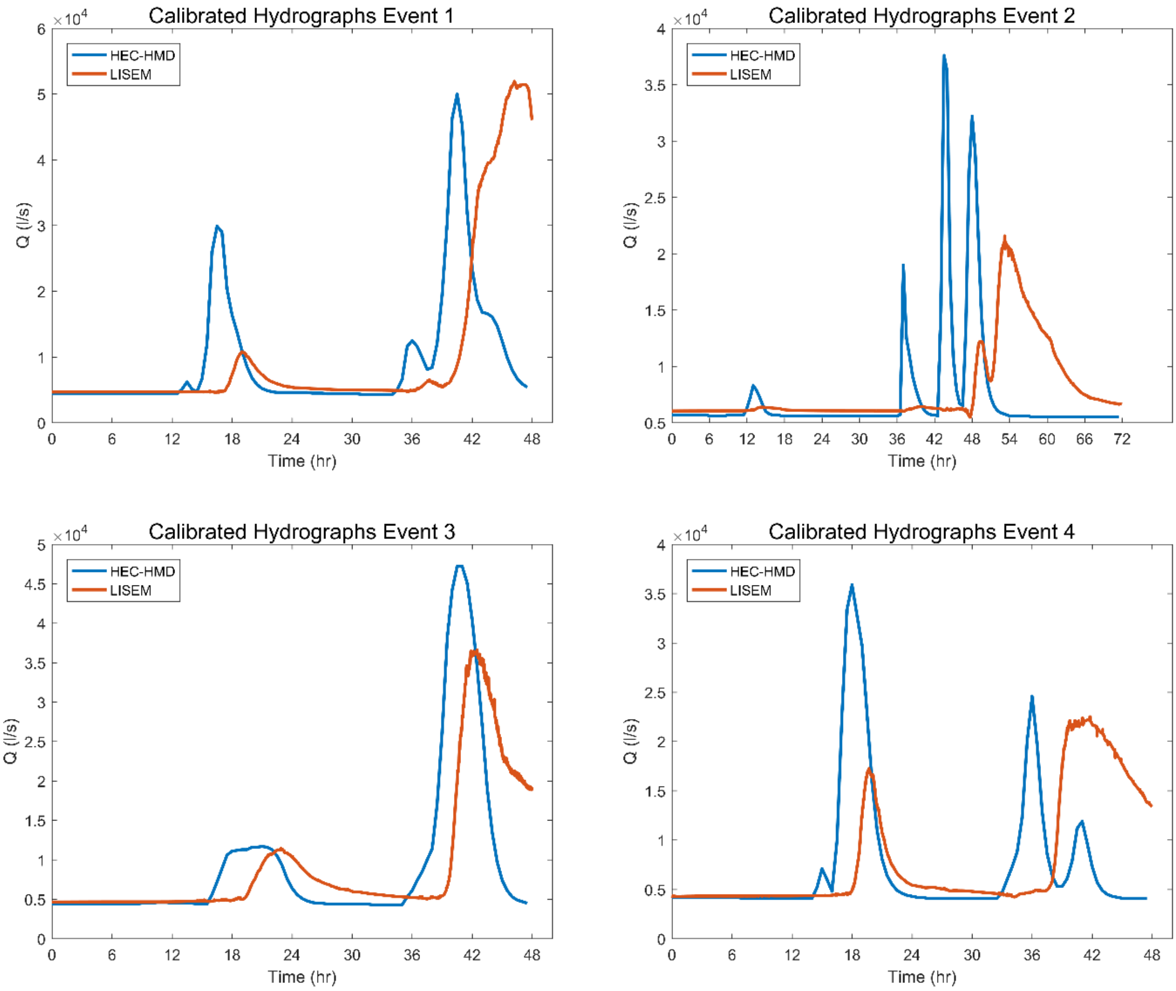

Figure 4.10 Hydrographs of four flooding events from HEC-HMS simulations and calibrated hydrographs from LISEM simulations.

The magnitudes of discharge obtained from two models are compared. Figure 4.11 shows the model performance by comparing total (RVE) and differences in peak discharge (Δ). As RVE is the first target in model calibration, the values of it are satisfying in all the events. As the second target, some poor values appear in the difference in the peak values. In Event 1, 2, and 4, LISEM is able to fit one of the two peaks, while the contrast of the other is quite considerable. In Event 2, LISEM failed to meet both two peaks. Compared to HEC-HSM, LISEM tends to offer a relatively smaller peak in the first storm and a larger one in the second storm. It can be explained by the principle of the model. Since rainfall is distributed in the whole area in LISEM, it is possible to create higher peaks only when the system is close to saturated, and a quick rise in the discharge sharply after a storm in avoided. However, this distribution is not considered in HEC-HMS model, so it is not possible to fit two discharge peaks at the same time.

Apart from that, almost all the RVE values except one are positive, while all the Δ values except one are negative, which shows a completely contrast feature. It also results from the difference in the model principle. The conversion from rainfall to runoff is much more direct in a lumped model than in a distributed model. Discharge drops immediately after reaching a peak in HEC-HSM if there is no more rainfall. However, the process is much more slowly in LISEM, which is easy to be observed in Figure 4.10. When the magnitudes of the peaks are the same, the total discharge of LISEM is higher.

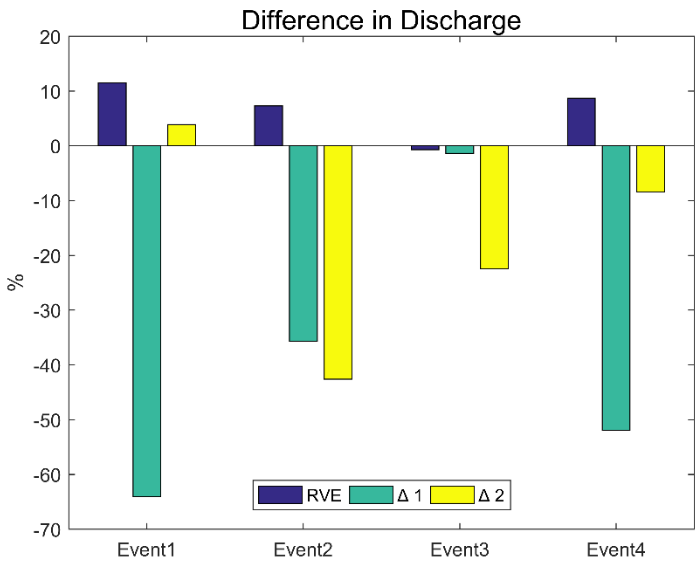

Figure 4.11 RVE and error Δ in the discharge of calibrated LISEM simulations compared to HEC-HMS simulations.

4.3.4. Inundated Area

After model calibration, the maximum water depths during the entire simulation period in four events are indicated in Figure 4.12. The maximum water depths simulated is small for events with no extensive and continuous inundated area simulated. Among the four events, very shallow water layer can be seen along the channel located in the southwest in Event 3.

Apart from that, a visible boundary is observed between the area with larger and smaller inundation. The boundary is consistent with that between CMORPH pixels, and more overland flow and inundation that is likely created in the area receiving more rainfall. It proves that rainfall has much more effects on water storage in local cells than distant cells in this case. It is because that rainwater always first infiltrates and saturates the soil layer in case rainfall intensity is lower than infiltration capacity. Some area with surface water storage and inundation is caused by local depressions since it has the similar distribution with that in the right map in Figure 4.7.

In general, most of the inundated area is created by rainfall and depressions at localized grid cells instead of larger scale flood inundation. The direct explanation is that the streamflow in the channel is does not exceed river banks to generate inundation flooding. In fact, it was found in the calibration process that a vast inundated area can be created when more runoff and thus higher discharges are simulated. Flooding mostly occurs in the flat region close to the outlet in the southwest part of the area. However, its corresponding simulated discharge would overtake the present one largely, and the performance in discharge simulation would worsen dramatically.

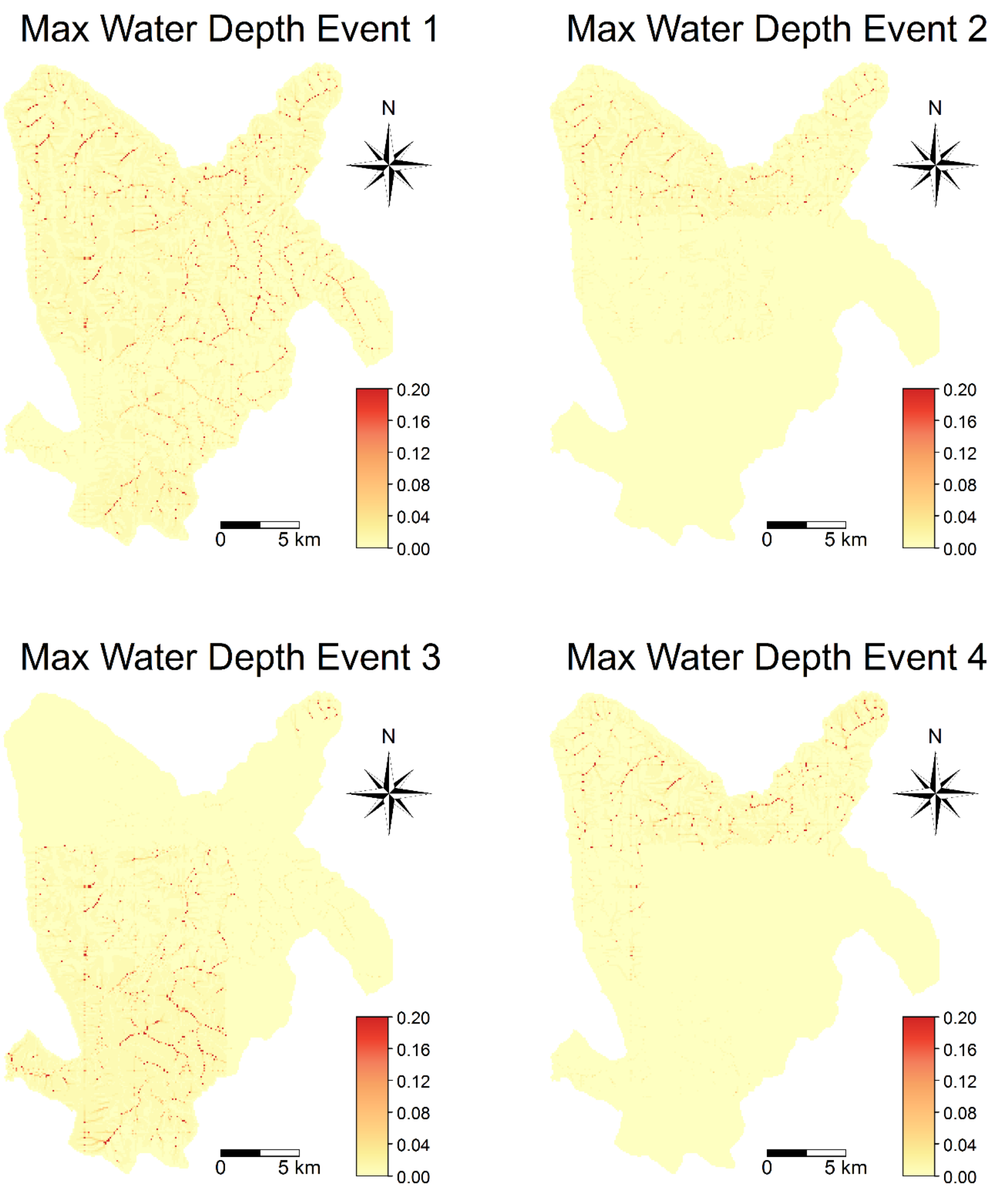

Figure 4.12 Maximum water depths during simulation period after calibration (Unit: m).

In contrast, the extensive inundated area was generated in the previous simulation by Manyifika (2015) suing SOBEK flood model with similar boundary conditions. The most considerable difference between inputs of these two studies is the area of simulation scale and the resolution of DEM map. The SOBEK model only simulated flooding in part of Kigali city, and the spatial resolution of it was from 10 to 20 m. Compared to that, LISEM was applied to a much more extensive area with much coarser resolution. Due to a large area, water in upstream part has to flow through a long distance before converging to the outlet, and the system would react slowly. The travel time of water from different locations also varies a lot, leading to a smoother peak discharge. Regarding the resolution, the length of a side in a cell is 90 m, the size is thus 8100 m^2. When water overflows from channels to land surface, the water depth is the mean value of a cell. Due to the large size of a cell, the amount of overflowing water can only generate a very shallow inundation depth. It is also noted that in LISEM simulation a large amount of water, in fact most of the rainfall, is consumed by means of infiltration. Therefore, the amount of water flowing into the downstream section of the main river is reduced considerably and is too little to create flooding.

4.4. Flood Forecasting

Flood forecasting procedure was operated with lead times from 12 to 48 hr. The forecasted hydrographs in Event 1, 3, and 4 were compared in Figure 4.13 (a). ECMWF forecasts combined with corrected CMORPH served as rainfall inputs in the model, and the principle is stated in Section 3.8. The time on the x-axis is from 12.00 to 24.00 on the second day of each event, which is the last 12 hr of the entire simulation period (48 hr in total). Since the variance among the forecasted graphs with different lead times in the beginning 36 hr is minimal, only the hydrographs during the last 12 hr of the simulation period are indicated.

In Event 1, none of the results succeeds to forecast the magnitude of the peak discharge. 48 hr forecasts substantially overestimate the discharge while the others largely underestimate it. The results become better in Event 3. The results with lead times of 12, 24, and 48 hr succeed to forecast the time of the peak though the value is not so accurate. In Event 4, 12 hr forecasts fit the hydrograph very well, while the others fail to forecast a massive amount of discharge.

The upper bar plot in Figure 4.13 (b) shows the total amount of rainfall from two products. The indicators on x-axis mean the accumulative rain values from ECMWF forecasts with different lead times and CMORPH estimates in the remaining period. The summation of one column is the total rainfall in one forecasting model run. ECMWF forecasts represent the rainfall at the unknown time (i.e., respective lead times), while CMORPH estimates represent the rainfall in the past time. In Event 1, ECMWF forecasts provide more rainfall in 48 hr forecasts and the opposite in the rest forecasts, which can be observed from the graphs. It is the same situation in Event 3 that 48 and 36 hr forecasts provide larger discharge due to larger meteorological inputs. Compared to CMOPRH, ECMWF underestimates the rainfall in forecasts with all the lead times in Event 4. However, the performance of 12 hr forecasts is still acceptable since it uses CMORPH data in the first 36 hr and the difference of rainfall in the last 12 hr is minimal.

In general, larger rainfall inputs lead to larger discharge as expected, which is reflected from Figure 4.13. However, the difference in the graphs seems to be much more significant than that in the rain values, especially in 48 hr forecast of Event 1 and 12 hr forecast in Event 4. Since only the graphs in the last 12 hr are indicated, the difference among the graphs is enlarged.

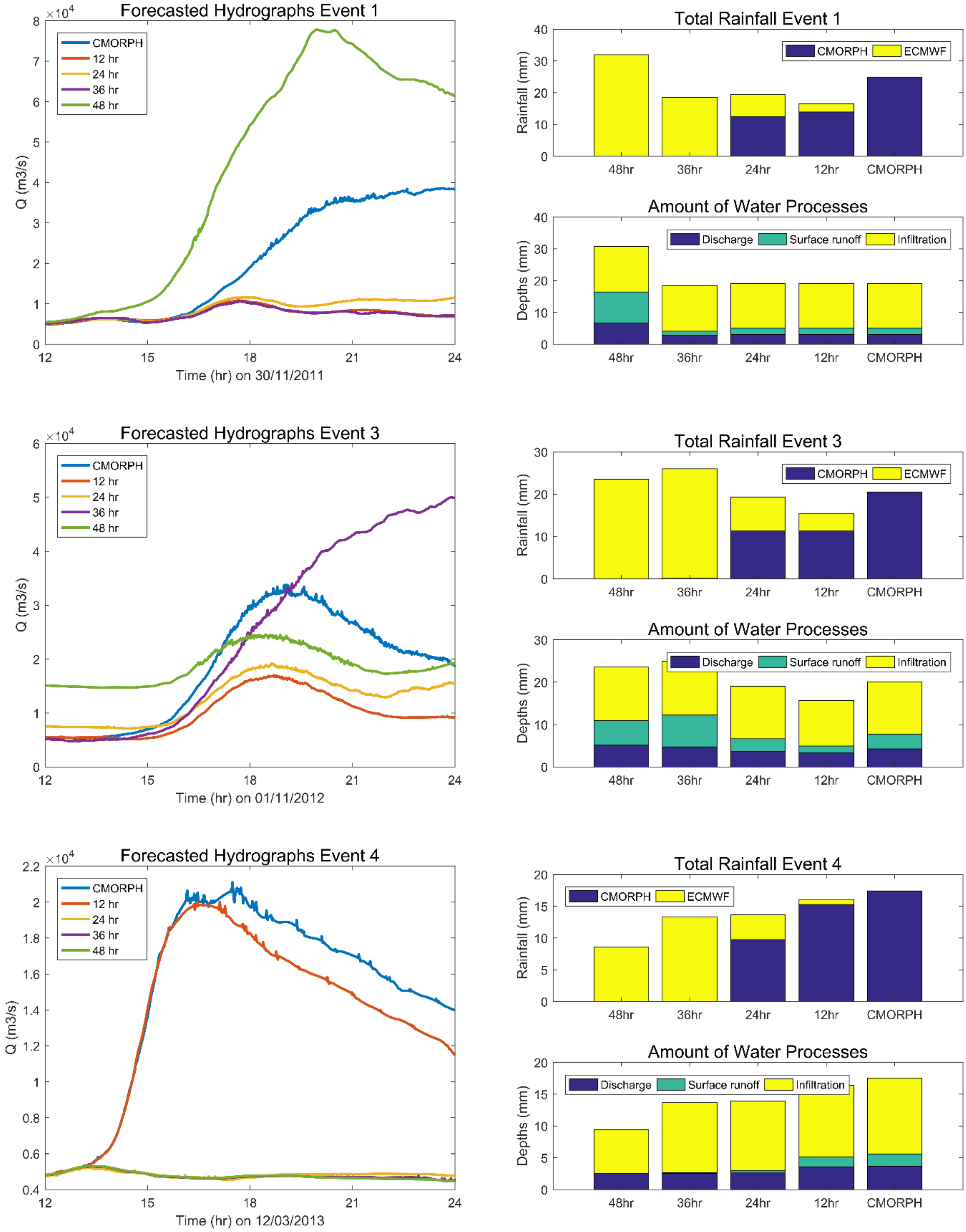

Figure 4.13 (a) Forecasted hydrographs obtained from ECMWF forecasts combined with corrected CMORPH in the last 12 hr of simulation. (b) Upper graphs show the accumulative rain values in two-day events. The summation of one column is the total rainfall in one forecasting run. Lower graphs show the amounts of water processes during the entire simulation period.

Another possible reason is reflected from the lower bar plot in Figure 4.13 (b). It shows the spatially average depths of discharge, surface runoff, and infiltration during the simulation period. Infiltration always shows the largest proportion, and the variance among infiltration is small as the soil layer is usually fully saturated at the end of the simulation. Therefore, the difference mainly lies in discharge and surface runoff, and the relative difference among discharge is more considerable due to its small base value. It reveals that the performance of flood forecasting can be hardly good unless very accurate precipitation forecasts are provided to LISEM, not only in the spatially average values but also in the spatially distributed patterns.

Usually, the accuracy of forecasting is supposed to increase as lead times decrease due to less uncertainty in rainfall forecasts. However, this is not precisely observed from the graphs. Forecasting skill score, in this case RMSE, also indicates the same feature apart from hydrographs. Table 4.3 lists the RMSE of all the forecasts. Within one event, RMSE does not always rise as the lead times rise. The performance of flood forecasts is determined mostly by the performance of ECMWF precipitation forecasts, and bias-corrected CMOPRH estimates are utilized to assess it. The uncertainty of CMOPRH product might be a reason for it since it cannot represent the rainfall in this area perfectly. The difference of both spatial and temporal resolution of these two rainfall products also makes the results less comparable. Despite that, the forecasting procedure in this study is distinct from a common one, which normally applies a much longer forecasting window (typically 5 to 15 days) and a longer interval (typically 1 day). In general, relatively reasonable results are still observed that the mean values of RMSE of the three events show a trend of rising with respect to the lead times. A more apparent trend is expected if a longer forecasting window and more events are selected.

Table 4.3 RMSE of discharge (m^3/s) in flood forecasting

	12 hr	24 hr	36 hr	48 hr
Event1	121.4	108.1	168.0	1132.1
Event3	325.4	1695.7	1371.9	12016.7
Event4	67.3	1553.7	1542.7	1537.9
Mean	171.4	1119.2	1027.5	4895.6

Figure 4.14 indicates the Maximum water depths during the entire simulation period of Event 3 with changing lead times. Event 3 was selected as the values of discharge from different forecasts are relatively closer to each other than in the other events. The variance in the inundation distribution can then reflect the effects of the spatially variable rainfall inputs. The hydrographs show larger discharge from 36 and 48 hr forecasts and smaller discharge from 12 and 24 hr forecasts. It is also reflected in Figure 4.14 that in the water depth images of 36 and 48 hr forecasts, larger discharge is corresponding to observed inundation in the entire area. In contrast, inundation can be only seen in the southwest part of the area in the water depth images of 12 and 24 hr forecasts.

Figure 4.13 (b) shows that 36 and 48 forecasts result entirely from ECMWF precipitation forecasts in Event 3, while 12 and 24 forecasts are more affected by CMORPH rainfall estimates. The distribution of inundated area is triggered by the distribution of the rainfall inputs. The separation between the area with and without inundation is due to the boundary of the CMORPH pixels with larger and smaller accumulative rainfall. ECMWF precipitation forecasts contain less spatial variance, thus the inundated area is spread over the entire area.

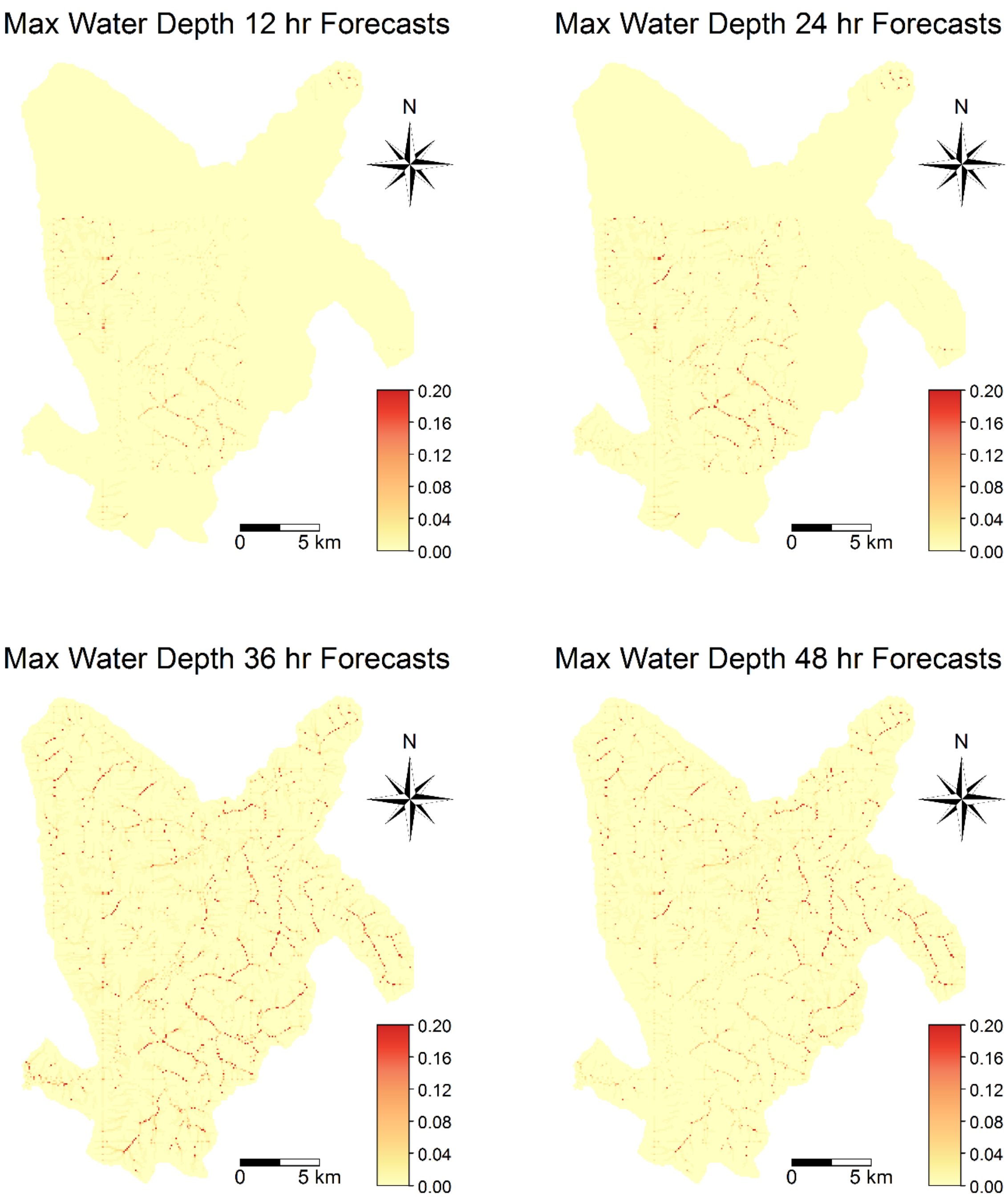

Figure 4.14 Maximum water depths during the entire simulation period of Event 3 when changing lead times from 12 to 48 hr are applied (Unit: m).

5. CONCLUSIONS AND RECOMMENDATIONS

5.1. Conclusions

In this study an integrated rainfall-runoff – inundation model and a flood forecasting procedure has been developed for Nyabugogo catchment and Kigali city in particular Four historical flooding events were simulated by use of OpenLISEM (version 3.96) software. A simple flood forecasting procedure was developed and tested with lead times from 12 to 48 hr. Bias corrected CMORPH rainfall estimates and ECMWF precipitation forecasts served as rainfall inputs. The research questions are answered below based on the study results.

- What bias correction scheme is the most effective for flood modelling purposes?
  In this study Time variable method proved to be the most effective bias correction scheme as it reduces the uncertainty in one rain gauge and is computed separately for each day. The tested length of time window (from 2 to 7 days) is indifferent to bias factors in most of the cases. The entire study area shares one factor, and most of the values are around 1.

- What are the most sensitive parameters and settings in the OpenLISEM model?
  In this study density of the channel network and the depths of soil layer proved to be the two most sensitive model settings for stream flow (i.e., channel flow) simulation, In the calibration process, initial moisture content is a very sensitive parameter, followed by Ksat of soil layer. However, all of them have an impact on only the magnitude but not as much on time the maximum discharge is simulated by the model.

- What is the performance of the model in simulating historical flooding events?
  The overall performance of the total streamflow simulation is good. The second peak discharge is always higher than the first one, since the rainfall intensities are too low to generate infiltration excess (i.e, Hortonian) overland flow. Any rise of soil moisture content leads to result in full saturation leads to s overland flow in the second peak. As a distributed model, the peak time delays more than compared to HEC-HMS, also duration of a peak flow time window is longer.

- What are the potentially inundated areas according to simulation?
  In general, most of the inundated area is created by high intense rainfall and depressions at localized grid cells instead of larger scale flooding in Kigali city area. Rainfall intensities provided by CMORPH estimates during flood events are too low to generate overland flow and thus rainfall does not directly converge to result in channel flow. Only when infiltration in the model is reduced to a very small value overland flow is generated. A such past observed real world catchment runoff behaviour and flood inundation could not be satisfactory simulated.

- What are the main sources of uncertainty in model development?
  The usage of CMORPH rainfall estimates and the selection of bias correction scheme can cause much uncertainty in meteorological conditions. The lack of in-situ measurements in the dimensions of the channels and the hydraulic properties of the soil is the main source of

uncertainty in terms of catchment characteristics. SRTM DEM map with a very coarse resolution also contains uncertainty in representing topography in the area.

- How to evaluate flood forecasting model performance?
  The performance of flood forecasting is evaluated by comparing the model results obtained from ECMWF precipitation forecasts to those from CMORPH estimates, which are considered as more representative rainfall inputs. In this study, total discharge estimates from two simulations during 12 hr in the flooding events are compared.

- How is flood forecasting performance affected by increasing forecasting lead times (12 to 48 hr)?
  The overall performance of forecasting is acceptable but not excellent that some forecasted hydrographs can fit the magnitude of discharge from simulation using corrected CMORPH rainfall estimates while the rest cannot. As lead times rise from 12 to 48 hr, the performance of the forecasts has a trend to worsen in terms of RMSE. However, it is not clearly observed due to the small number of the tested events.

- How does the uncertainty in rainfall forecasts affect the accuracy of flood forecasting?
  Rainfall forecasts are the deterministic factors in flood forecasting. It seems that the peak discharge is not possible to be forecasted unless ECMWF provides very accurate precipitation forecasts. The spatial patterns of rainfall inputs are essential as well in LISEM simulation. Since the spatial resolution of the two used rainfall products is largely different, the forecasts on the inundated area are not very reliable.

In conclusion, the OpenLISEM is capable of simulating outlet discharge during a flooding event in this study, but the performance of inundation simulation is not very satisfying. The most prominent cause is the manner overland is generated under the condition that rainfall intensity is higher than infiltration capacity by the Green-Ampt approach. Secondly, a relatively coarse spatial resolution (i.e., grid resolution) is used in this study that directly affects the representation of floodplain elevations and slopes. The performance of flood forecasting is moderate in forecasting discharge with lead times from 12 to 48 hr.

5.2. Recommendations

The biggest obstacle in this study is the lack of in-situ data which, if available, is of poor quality. More densely distributed rain gauges with continuous rainfall records are more representative rainfall inputs is needed for flood modelling purposes in this catchment. Moreover, more in-situ measurements in catchment characteristics, mainly including distribution and dimensions of channels, hydraulic properties of soil, and topography in the urban area, are required for further study on flood analysis. Lastly, it is preferred to use rainfall-runoff models that also allow for simulation of ground water flow driven saturation excess overland flow and interflow/rapid subsurface flow processes.

LIST OF REFERENCES

Ali, H. T. (2016). *Digital urban terrain characterization for 1D2D hydronamic flood modelling in Kigali, Rwanda (MSc thesis).*

Baartman, J. E. M., Jetten, V. G., Ritsema, C. J., & de Vente, J. (2012). Exploring effects of rainfall intensity and duration on soil erosion at the catchment scale using openLISEM: Prado catchment, SE Spain. *Hydrological Processes*, *26*(7), 1034–1049. https://doi.org/10.1002/hyp.8196

Batjes, N. H. (1997, March). A world dataset of derived soil properties by FAOGÇôUNESCO soil unit for global modelling. *Soil Use and Management*. https://doi.org/DOI 10.1111/j.1475-2743.1997.tb00550.x

Benninga, H. F. (2015). *Performance and limitations of ensemble river flow forecasts*.

Bizimana, J. P., & Schilling, M. (2010). Geospatial Techniques in Urban Hazard and Disaster Analysis. *Geospatial Techniques in Urban Hazard and Disaster Analysis*, *2*(February 2016), 99–124. https://doi.org/10.1007/978-90-481-2238-7

Bout, B., & Jetten, V. G. (2018). The validity of flow approximations when simulating catchment-integrated flash floods. *Journal of Hydrology*, *556*, 674–688. https://doi.org/10.1016/j.jhydrol.2017.11.033

Buizza, R., Houtekamer, P. L., Pellerin, G., Toth, Z., Zhu, Y., & Wei, M. (2005). A Comparison of the ECMWF, MSC, and NCEP Global Ensemble Prediction Systems. *Monthly Weather Review*, *133*(5), 1076–1097. https://doi.org/10.1175/MWR2905.1

Chow, V. Te. (1959). *Open-Channel Hydraulics*. https://doi.org/ISBN 07-010776-9

Cosgrove, W. J., & Rijsberman, F. R. (2014). *World Water Vision, Making water everybod's business. Chaprter 1. Earthscan Publications*. London: Taylor and Francis. https://doi.org/10.1017/CBO9781107415324.004

de Jong, S. M., & Jetten, V. G. (2007). Estimating spatial patterns of rainfall interception from remotely sensed vegetation indices and spectral mixture analysis. *International Journal of Geographical Information Science*, *21*(5), 529–545. https://doi.org/10.1080/13658810601064884

de Roo, A. P. J., Wesseling, C. G., & Ritsema, C. J. (1996). LISEM: a single-event pysically based hydrological and soil erosion model for drainage basins.I: theroy, input and output. *Hydrological Processes*, *10*(8), 1107–1117. https://doi.org/10.1002/(SICI)1099-1085(199608)10:8<1107::AID-HYP415>3.0.CO;2-4

ECMWF Directorate. (2012). Describing ECMWF's forecasts and forecasting system. *ECMWF Newletter*, pp. 11–13. https://doi.org/10.21957/6a4lel9e

Fujisada, H., Bailey, G. B., Kelly, G. G., Hara, S., & Abrams, M. J. (2005). ASTER DEM performance. *IEEE Transactions on Geoscience and Remote Sensing*, *43*(12), 2707–2713. https://doi.org/10.1109/TGRS.2005.847924

Green, W. H., & Ampt, G. (1911). Studies on soil physics, 1. The flow of air and water through soils. *Journal of Agricultural Science*, *4*(82), 1–24.

Habib, E., Haile, A. T., Sazib, N., Zhang, Y., & Rientjes, T. (2014). Effect of bias correction of satellite-rainfall estimates on runoff simulations at the source of the Upper Blue Nile. *Remote Sensing*, *6*(7), 6688–6708. https://doi.org/10.3390/rs6076688

Habonimana, H. V. (2014). *Integrated Flood Modeling In Lubigi Catchment Kampala*.

Habonimana, H. V., Bizimana, J. P., Uwayezu, E., & Tuyishimire, J. (2012). Integrated flood modeling for flood hazard assessment in Kigali City , Rwanda.

Haile, A. T., Habib, E., & Rientjes, T. (2013). Evaluation of the climate prediction center (CPC) morphing technique (CMORPH) rainfall product on hourly time scales over the source of the Blue Nile River.

Hydrological Processes, *27*(12), 1829–1839. https://doi.org/10.1002/hyp.9330

Haile, A. T., Tefera, F. T., & Rientjes, T. (2016). Flood forecasting in Niger-Benue basin using satellite and quantitative precipitation forecast data. *International Journal of Applied Earth Observation and Geoinformation*, *52*, 475–484. https://doi.org/10.1016/j.jag.2016.06.021

Hengl, T., Mendes de Jesus, J., Heuvelink, G. B. M., Ruiperez Gonzalez, M., Kilibarda, M., Blagotić, A., … Kempen, B. (2017). SoilGrids250m: Global gridded soil information based on machine learning. *PLOS ONE*, *12*(2), e0169748. https://doi.org/10.1371/journal.pone.0169748

Hirano, A., Welch, R., & Lang, H. (2003). Mapping from ASTER stereo image data: DEM validation and accuracy assessment. In *ISPRS Journal of Photogrammetry and Remote Sensing* (Vol. 57, pp. 356–370). https://doi.org/10.1016/S0924-2716(02)00164-8

Horritt, M. S., Di Baldassarre, G., Bates, P. D., & Brath, A. (2007). Comparing the performance of a 2-D finite element and a 2-D finite volume model of floodplain inundation using airborne SAR imagery. *Hydrological Processes*, *21*(20), 2745–2759. https://doi.org/10.1002/hyp.6486

Jarihani, A. A., Callow, J. N., McVicar, T. R., Van Niel, T. G., & Larsen, J. R. (2015). Satellite-derived Digital Elevation Model (DEM) selection, preparation and correction for hydrodynamic modelling in large, low-gradient and data-sparse catchments. *Journal of Hydrology*, *524*, 489–506. https://doi.org/10.1016/j.jhydrol.2015.02.049

Jetten, V., & van den Bout, B. (2017). LISEM Limburg Soil Erosion model v 3.9x: Documentation & User Manual.

Jolliffe, I. T., & Stephenson, D. B. (2003). *Forecast Verification: A Practitioner's Guide in Atmospheric Science. Wiley*. https://doi.org/10.1016/j.ijforecast.2005.11.002

Jones, P. G., & Thornton, P. K. (2015). Representative soil profiles for the Harmonized World Soil Database at different spatial resolutions for agricultural modelling applications. *Agricultural Systems*, *139*, 93–99. https://doi.org/10.1016/j.agsy.2015.07.003

Krzhizhanovskaya, V. V., Shirshov, G. S., Melnikova, N. B., Belleman, R. G., Rusadi, F. I., Broekhuijsen, B. J., … Meijer, R. J. (2011). Flood early warning system: Design, implementation and computational modules. In *Procedia Computer Science* (Vol. 4, pp. 106–115). https://doi.org/10.1016/j.procs.2011.04.012

Manyifika, M. (2015). *Diagnostic assessment on urban floods using satellite data and hydrologic models in Kigali, Rwanda. ITC Thesis.*

Mark, O., Weesakul, S., Apirumanekul, C., Aroonnet, S. B., & Djordjević, S. (2004). Potential and limitations of 1D modelling of urban flooding. *Journal of Hydrology*. https://doi.org/10.1016/j.jhydrol.2004.08.014

Mein, R. G., & Larson, C. L. (1971). *Modeling the Infiltration Component of the Rainfall-runoff Process.*

Mhonda, A. (2013). *Evaluating Flash Flood Risk Reduction Strategies in Built-up Environment in Kampala Evaluating Flash Flood Risk Reduction Strategies in Built-up Environment in Kampala. Enschede, ITC.*

Mignot, E., Paquier, A., & Haider, S. (2006). Modeling floods in a dense urban area using 2D shallow water equations. *Journal of Hydrology*, *327*(1–2), 186–199. https://doi.org/10.1016/j.jhydrol.2005.11.026

Mwendera, E. J., & Feyen, J. (1992). Estimation of depression storage and Manning's resistance coefficient from random roughness measurements. *Geoderma*, *52*(3–4), 235–250. https://doi.org/10.1016/0016-7061(92)90039-A

Noto, L. V., Ivanov, V. Y., Bras, R. L., & Vivoni, E. R. (2008). Effects of initialization on response of a fully-distributed hydrologic model. *Journal of Hydrology*, *352*(1–2), 107–125. https://doi.org/10.1016/j.jhydrol.2007.12.031

Onstad, T. M. Z. and C. A. (1987). Tillage and rainfall effects on random roughnes：A review.pdf, *9*, 1–20.

Pcraster Team. (2011). PCRaster Documentation.

Rawls, W. J., Brakensiek, D. L., & Miller, N. (1983). Green-ampt Infiltration Parameters from Soils Data. *Journal of Hydraulic Engineering*, *109*(1), 62–70. https://doi.org/10.1061/(ASCE)0733-9429(1983)109:1(62)

Rientjes, T. (2015). Hydrologic modelling for Intergated Water Resource. *Lecture Notes for WREM, ITC/University of Twente*.

Rodriguez, E., Morris, C. C., & Belz, J. J. (2006). A global assessment of the SRTM performance. *Photogrammetric Engineering and Remote Sensing*, *72*(3), 249–260. https://doi.org/10.14358/PERS.72.3.249

Romang, H., Zappa, M., Hilker, N., Gerber, M., Dufour, F., Frede, V., … Rhyner, J. (2011). IFKIS-Hydro: An early warning and information system for floods and debris flows. *Natural Hazards*, *56*(2), 509–527. https://doi.org/10.1007/s11069-010-9507-8

Roulin, E., & Vannitsem, S. (2005). Skill of Medium-Range Hydrological Ensemble Predictions. *Journal of Hydrometeorology*, *6*(5), 729–744. https://doi.org/10.1175/JHM436.1

Saxton, K. E., & Rawls, W. J. (2006). Soil Water Characteristic Estimates by Texture and Organic Matter for Hydrologic Solutions. *Soil Science Society of America Journal*, *70*(5), 1569. https://doi.org/10.2136/sssaj2005.0117

Schumann, G., Matgen, P., Cutler, M. E. J., Black, A., Hoffmann, L., & Pfister, L. (2008). Comparison of remotely sensed water stages from LiDAR, topographic contours and SRTM. *ISPRS Journal of Photogrammetry and Remote Sensing*, *63*(3), 283–296. https://doi.org/10.1016/j.isprsjprs.2007.09.004

Sendama, M. I. (2015). *Assessment of Meteorological Remote Sensing Products for Stream Flow Modelling Using HBV-light in Nyabarongo Basin , Rwanda. ITC Thesis..*.

Sliuzas, R., Flacke, J., & Jetten, V. (2013). Modelling Urbanization and Flooding in Kampala,Uganda. *N-Aerus.Net*, (September). https://doi.org/N-AERUS XIV

Soil Water Characteristics. (n.d.). Retrieved October 2, 2017, from https://www.nrcs.usda.gov/wps/portal/nrcs/detailfull/national/water/?cid=stelprdb1045311

Strahler, A. N. (1952). Hypsometric (Area - Altitude) Analysis of Erosional Topography. *Geological Society of America Bulletin*, *63*(11), 1117–1142. https://doi.org/10.1130/0016-7606(1952)63

UNISDR. (2002). *Guidelines for Reducing Flood Losses. United Nations - Headquarters (UN), available on-line at: https://www.unisdr.org/we/inform/publications/558*.

Van Zyl, J. J. (2001). The shuttle radar topography mission (SRTM): A breakthrough in remote sensing of topography. In *Acta Astronautica* (Vol. 48, pp. 559–565). https://doi.org/10.1016/S0094-5765(01)00020-0

West Sacramento City Hall. (2002). Standard Specifications and Details, Storm Drainage.